

AD-A070 348

MICROWAVE ASSOCIATES INC BURLINGTON MASS
HIGH MICROWAVE FREQUENCY PASSIVE COMPONENTS.(U)
JUN 77 C BUNTSCHUH

F/6 9/5

N00173-76-C-0313

NL

UNCLASSIFIED

| OF |
AD
A070348



① LEVEL II
SC

AD A 070348

FINAL REPORT

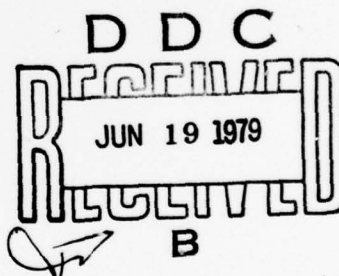
HIGH MICROWAVE FREQUENCY PASSIVE COMPONENTS

Prepared by
Charlie Buntschuh

APPROVED FOR PUBLIC RELEASE
DISTRIBUTION UNLIMITED

Microwave Associates, Inc.
Burlington, MA 01803

Program Sponsored By Office Of Naval Research
Department Of The Navy
Arlington, VA



DDC FILE COPY

Microwave Associates, Inc.
Final Report.
HIGH MICROWAVE FREQUENCY PASSIVE
COMPONENTS.
57 pgs., June 3, 1977

NRL 542238

UNCLASSIFIED

Copy # (Rec'd) Date
1--5-31-79

Copy # (Dest) Date

N00173-76-C-0313
(NRL Contract)

5-25-79
new

79 06 04 061

9 Final rept. 30 Aug 76-11 Mar 77

SECURITY CLASSIFICATION OF THIS PAGE (When Data Entered)

| REPORT DOCUMENTATION PAGE | | READ INSTRUCTIONS BEFORE COMPLETING FORM |
|---|-----------------------|--|
| 1. REPORT NUMBER | 2. GOVT ACCESSION NO. | 3. RECIPIENT'S CATALOG NUMBER |
| 4. TITLE (and Subtitle) Final Report High Microwave Frequency Passive Components | | 5. TYPE OF REPORT & PERIOD COVERED Final, 8/30/76-3/11/77 |
| 7. AUTHOR(s) Dr. Charles Buntschuh | | 6. PERFORMING ORG. REPORT NUMBER |
| 9. PERFORMING ORGANIZATION NAME AND ADDRESS Microwave Associates, Inc. Burlington, MA 01803 | | 8. CONTRACT OR GRANT NUMBER(s) N00173-76-C-0313 |
| 11. CONTROLLING OFFICE NAME AND ADDRESS Office of Naval Research Arlington, VA | | 10. PROGRAM ELEMENT, PROJECT, TASK AREA & WORK UNIT NUMBERS 11/3 Jun 77 |
| 14. MONITORING AGENCY NAME & ADDRESS (if different from Controlling Office) Naval Research Laboratory 4555 Overlook Drive Washington, DC 20375 | | 12. REPORT DATE June 3, 1977 |
| | | 13. NUMBER OF PAGES 57 |
| | | 15. SECURITY CLASS. (of this report) Unclassified |
| 16. DISTRIBUTION STATEMENT (of this Report) Reproduction in whole or in part is permitted for any purpose of the United States Government DISTRIBUTION STATEMENT A Approved for public release; Distribution Unlimited | | 18a. DECLASSIFICATION/DOWNGRADING SCHEDULE |
| 17. DISTRIBUTION STATEMENT (of the abstract entered in Block 20, if different from Report) | | |
| 18. SUPPLEMENTARY NOTES | | |
| 19. KEY WORDS (Continue on reverse side if necessary and identify by block number) Microstrip, attenuators, mixers, microwave integrated circuits, frequency converters. | | |
| 20. ABSTRACT (Continue on reverse side if necessary and identify by block number) The report describes the design and development of the RF sections of a frequency translator and a linear amplitude modulator for high band, similar to units developed for low band on Contract N00014-74-C-0066 and N0014-75-C-0814. | | |

continued...

DD FORM 1473

1 JAN 73

EDITION OF 1 NOV 65 IS OBSOLETE

Unclassified

SECURITY CLASSIFICATION OF THIS PAGE (When Data Entered)

229 400

50B

Unclassified

SECURITY CLASSIFICATION OF THIS PAGE(When Data Entered)

The microwave integrated circuits developed were principally alumina microstrip. Preliminary experiments on stripline components are also described.

Final performance data on the translator and modulator are given and discussed.

| | |
|--------------------|--|
| Accession For | |
| NTIS GRA&I | <input checked="checked" type="checkbox"/> |
| DDC TAB | <input type="checkbox"/> |
| Unannounced | <input type="checkbox"/> |
| Justification | |
| By | |
| Distribution/ | |
| Availability Codes | |
| Dist | Avail and/or special |
| A | |

Unclassified

SECURITY CLASSIFICATION OF THIS PAGE(When Data Entered)

FINAL REPORT

HIGH MICROWAVE FREQUENCY PASSIVE COMPONENTS

Prepared by
C. Buntschuh

Microwave Associates, Inc.
Burlington, MA 01803

Program Sponsored By Office Of Naval Research
Department Of The Navy
Arlington, VA

Contract No. N00173-76-C-0313

TABLE OF CONTENTS

| | <u>Page</u> |
|---|-------------|
| 1. INTRODUCTION | 1 |
| 1.1 Program Objectives | 1 |
| 1.2 Frequency Translator | 2 |
| 1.3 Linear Amplitude Modulator | 5 |
| 1.4 Organization of Presentation | 9 |
| 2. COMPONENT DEVELOPMENT | 10 |
| 2.1 Discussion of Transmission Line Media | 10 |
| 2.2 3-dB Hybrids | 13 |
| 2.3 In-Phase Power Dividers | 20 |
| 2.4 Bias Tee for Frequency Translator | 25 |
| 2.5 Frequency Translator Baseband Modulator | 28 |
| 2.6 Linear Modulator Driver | 30 |
| 3. FREQUENCY TRANSLATOR | 33 |
| 3.1 Theory | 33 |
| 3.2 Layout and Construction | 39 |
| 3.3 Performance Data | 42 |
| 4. LINEAR AMPLITUDE MODULATOR | 46 |
| 4.1 Design Considerations | 46 |
| 4.2 Layout and Construction | 48 |
| 4.3 Performance Data | 48 |
| 5. CONCLUSIONS AND RECOMMENDATIONS | 46 |

LIST OF ILLUSTRATIONS

| <u>Figure</u> | | <u>Page</u> |
|---------------|---|-------------|
| 1.2.1 | Schematic Diagram of RF Section of Frequency Translator | 3 |
| 1.2.2 | Block Diagram of Baseband Modulator Section of Frequency Translator | 4 |
| 1.3.1 | Balanced Linear Amplitude Modulator Schematic | 7 |
| 1.3.2 | Simplified Block/Schematic Diagram of LAM Driver | 8 |
| 2.2.1 | Measured Responses of 3-Section, Tandem 8.34 dB Microstrip 3-dB Hybrid on .020" Alumina | 14 |
| 2.2.2 | Measured Responses of 3-Section, 3-dB Stripline Coupler with .130" Ground Plane Spacing | 15 |
| 2.2.3 | Measured Responses of 3-Section 3 dB Stripline Coupler with .065" Ground Plane Spacing | 17 |
| 2.2.4 | Measured Responses of 3-Section, Tandem 8.34 dB Microstrip 3-dB Hybrid on .015" Alumina | 19 |
| 2.3.1 | Responses of Microstrip In-Phase Power Divider with Chip Resistors | 21 |
| 2.3.2 | Responses of Microstrip In-Phase Power Divider with Etched Resistors | 22 |
| 2.3.3 | Responses of Stripline In-Phase Power Divider | 24 |
| 2.4.1 | Dual Bias Lead Test Circuit | 26 |
| 2.4.2 | Characteristics of Dual Bias Lead Test Circuit | 27 |
| 2.5.1 | Baseband Modulator Input Driver and RC Phase Shift Network Topology | 29 |

LIST OF ILLUSTRATIONS
(cont'd)

| <u>Figure</u> | | <u>Page</u> |
|---------------|---|-------------|
| 2.5.2 | Baseband Modulator Output Driver | 31 |
| 2.6.1 | Modulator Driver Schematic | 32 |
| 3.1.1 | Ideal Resistive Mixer Sideband Generator | 34 |
| 3.1.2 | PIN Modulator Diode Reflection Coefficient vs DC Bias Voltage | 36 |
| 3.1.3 | Calculated Conversion Loss and Third Harmonic Suppression vs PIN Diode AC Drive Level | 37 |
| 3.1.4 | Relationship of Translator Performance to Circuit Characteristics | 38 |
| 3.2.1 | Frequency Translator Mixer Circuit Layout | 40 |
| 3.2.2 | High Band Frequency Translator | 41 |
| 3.3.1 | High Band Frequency Translator Conversion Gain and Carrier Suppression | 43 |
| 3.3.2 | High Band Frequency Translator Third Order and Unwanted First Order Sideband Suppression | 44 |
| 4.2.1 | High Band Linear Amplitude Modulator | 49 |
| 4.3.1 | Linear Amplitude Modulator Attenuation Characteristics | 50 |
| 4.3.2 | Linear Amplitude Modulator VSWR Characteristics | 51 |
| 4.3.3 | Linear Amplitude Modulator Attenuation vs Drive Signal | 53 |
| 4.3.4 | LAM Linearity Error vs Driver Input Voltage | 54 |
| 4.3.5 | LAM Switching Transient | 55 |

1. INTRODUCTION

1.1 Program Objectives

The objective of this program was to develop a frequency translator and linear amplitude modulator for the high band similar to the low band units developed on Contracts N00014-74-C-0066 and N00014-75-C-0814.

The RF circuits of the low band translator and modulator were 0.025" alumina microstrip. These circuits were adequate with respect to loss coupler directivity and match. We recognized that these parameters would inevitably degrade on moving to the high band, and some cognizance was taken of this in the high band performance specifications. We expected that it would be possible to translate the low band microstrip designs to the higher frequency using thinner alumina substrates. Nevertheless, we felt that alternate approaches should be explored from the outset to ensure success. Thus, a second objective was to experiment with other transmission line media for some of the basic circuit components in the translator and modulator.

The baseband modulator for the frequency translator and the driver for the linear amplitude modulator, developed on the second low band contract, performed quite satisfactorily. Since the designs of these units are independent of the RF frequency, we used the same designs, with only minor packaging changes, on the high band components. This contract did not include any further driver development.

1.2 Frequency Translator

The frequency translator takes an input microwave carrier frequency and shifts it either up or down by an offset frequency in the audio range.

The design requirements and specifications for the High Band Frequency Translator are the following:

| | |
|------------------------------|----------------------------|
| Bandwidth: | High Band Baseband |
| Conversion Loss: | 12 dB maximum, 10 dB, goal |
| Carrier Suppression: | 13 dB minimum |
| Unwanted Sideband Rejection: | 15 dB minimum |
| Spurious Sideband Rejection: | 15 dB minimum |
| RF Input Power: | 100 mW CW, maximum |
| Operating Temperature Range: | Room to 80°C |
| RF Connectors: | SMA Jack |

The unit must be capable of upward and downward translation, with the direction selectable by application of a control voltage.

The translator design concept is the same as that of the low band translator, modified as appropriate for the higher RF frequency. The translator is composed of an RF section and a baseband modulator section, as diagrammed in Figures 1.2.1 and 1.2.2. The RF section is an image out phasing single-sideband modulator using balanced mixer configurations. Its basic circuit elements are an in-phase power divider, three 3-dB quadrature hybrid couplers, and four modulator diode mounts with baseband

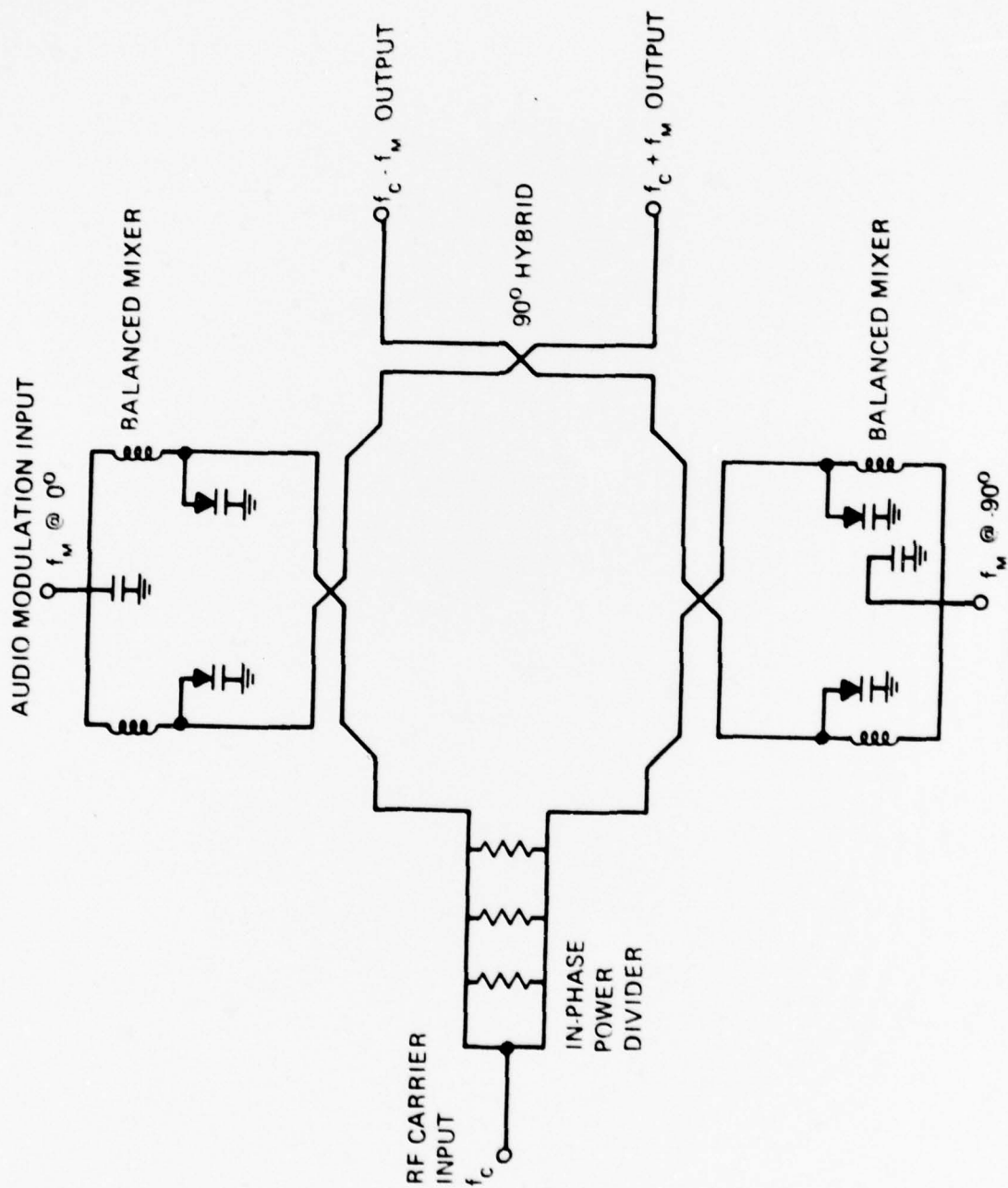


FIGURE 1.2.1 SCHEMATIC DIAGRAM OF RF SECTION OF FREQUENCY TRANSLATOR

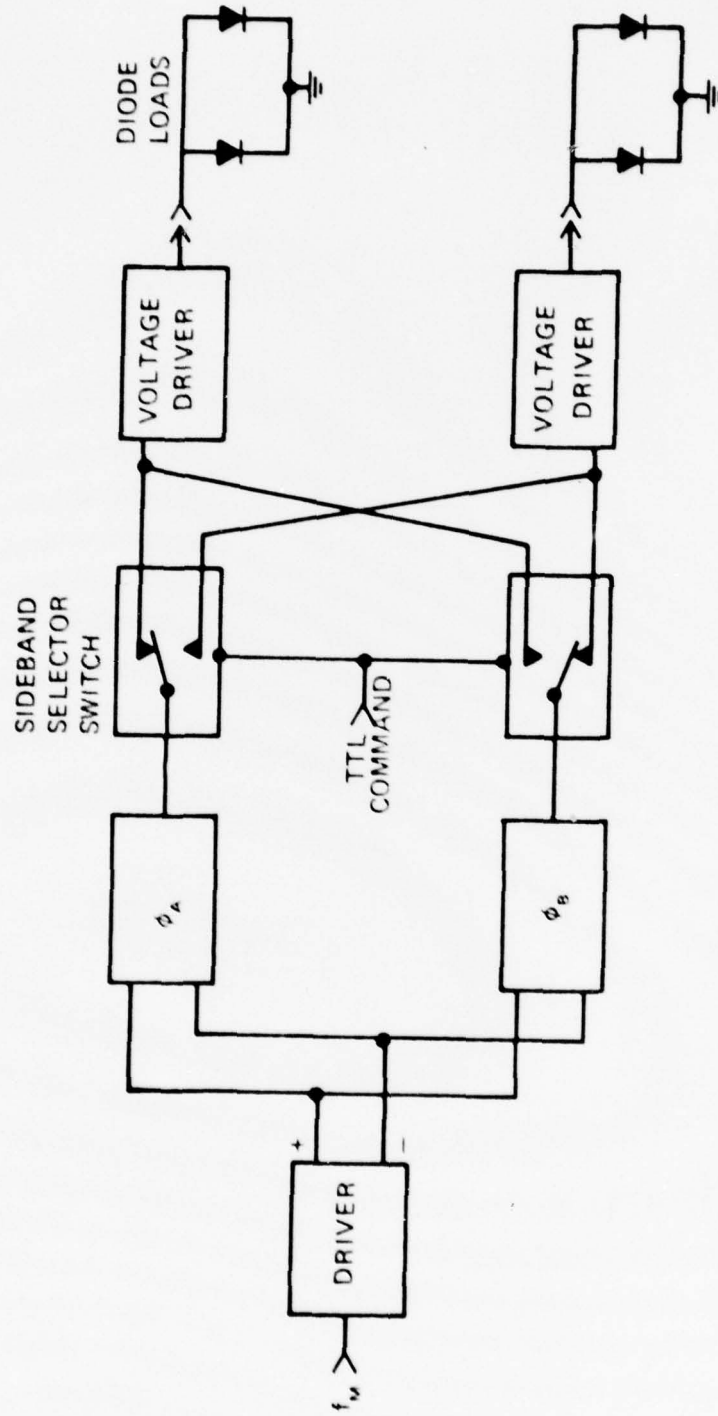


FIGURE 1.2.2 BLOCK DIAGRAM OF BASEBAND MODULATOR SECTION OF FREQUENCY TRANSLATOR

filter networks. The baseband modulator consists of a driver, a pair of phase shifting networks capable of operation over a three decade bandwidth, and a selector switch. Its input is a sinusoidal voltage at the modulation or offset frequency.

1.3 Linear Amplitude Modulator

The design requirements and specifications for the high band linear amplitude modulator are as follows:

| | |
|-------------------------------|---|
| Bandwidth: | High Band |
| Dynamic Range: | 45 dB minimum |
| Insertion Loss | 3.5 dB maximum, 2.0 dB goal |
| Attenuation Flatness: | ± 1.0 dB maximum ± 0.5 dB goal @ ≤ 10 dB attenuation. $\pm 10\%$ maximum $\pm 5\%$ goal @ ≥ 10 dB attenuation. |
| VSWR: | 2.0:1 maximum |
| Power Handling: | 3W CW maximum |
| Modulation Rate: | 1. MHz |
| Switching Time: | 60 ns maximum |
| DC and Video to RF Isolation: | 50 dB minimum |
| DC Power: | +10V only, desirable |
| Control Voltage: | 0-5V |
| Linearity: | 9 dB/volt ± 1 dB |
| Operating Temperature Range: | Room to 80°C |
| RF Connectors: | SMA jack |

The VSWR and bandwidth requirements dictated the use of the matched attenuator configuration, shown schematically in Figure 1.3.1. This is also the same configuration used at low band. The same 3-dB quadrature hybrid developed for the frequency translator are used in the modulator.

In the low band modulator the diode arms each consisted of four short 0.025" thick, alumina microstrip 50 ohm lines, with the shunt diodes mounted on the housing floor in the gaps between the alumina tiles. We had originally proposed to investigate this same construction as well as a TFG (Duroid) microstrip approach. The advantage of this is that the diodes could readily be shunt-mounted by removing the dielectric at the appropriate points so that only one circuit board is needed for each arm. Furthermore, since the Duroid substrate is approximately the same thickness as the diodes (0.007"), the diode bonding strap inductance could be minimized. Because of these conveniences, we immediately adopted the Duroid microstrip approach and did not attempt to use alumina microstrip for the diode arms.

The modulator driver consists of a linearizing network, a leading edge spiking circuit, and a trailing edge spiking circuit, as indicated in Figure 1.3.2. The single breakpoint adjusts the long term diode current to such values that the RF attenuation is approximately proportional to the input command voltage. The spiking circuits apply overvoltage pulses to the diode--proportional to the command voltage on the leading edge and a fixed amplitude on the trailing edge--to speed up the switching transients.

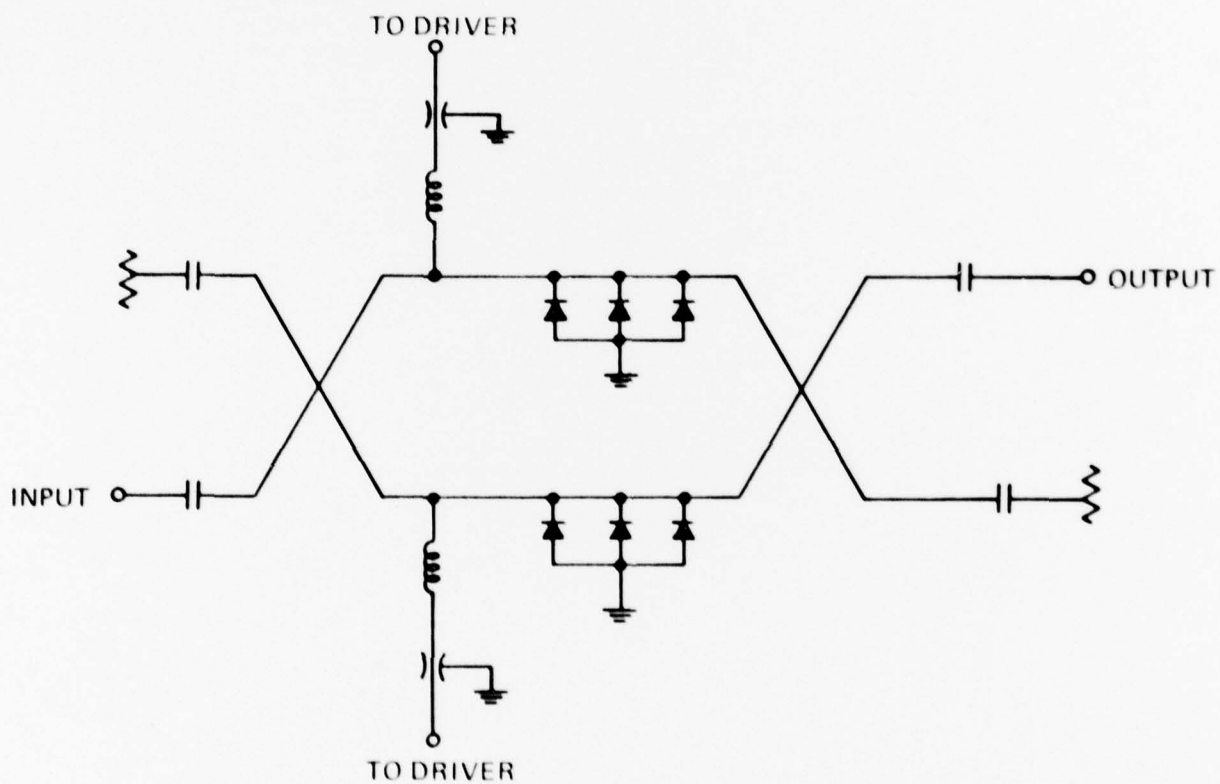


FIGURE 1.3.1 BALANCED LINEAR AMPLITUDE MODULATOR SCHEMATIC

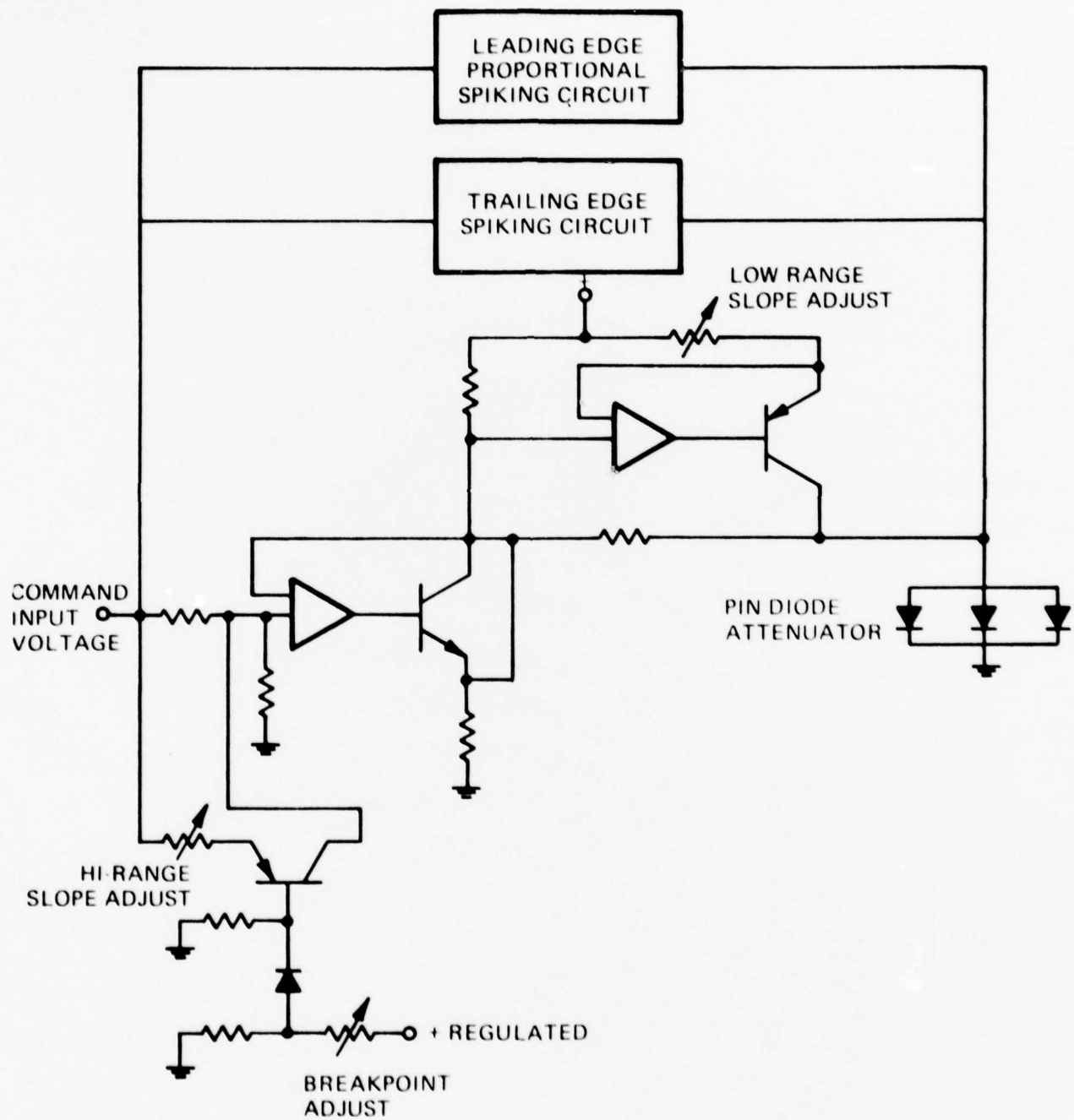


FIGURE 1.3.2 SIMPLIFIED BLOCK/SCHEMATIC DIAGRAM OF LAM DRIVER

1.4 Organization of Presentation

In Section 2 we summarize the development work on the principal circuit components. In particular it describes and compares the results on microstrip and stripline 3-dB hybrids and in-phase power dividers. Section 3 covers the frequency translator, including its theory of operation and the performance data on the unit built. The linear modulator is similarly described in Section 4, and Section 5 contains the conclusions and recommendations.

2. COMPONENT DEVELOPMENT

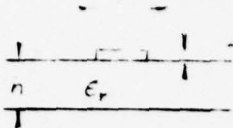
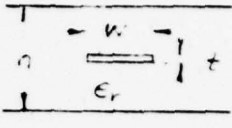
2.1 Discussion of Transmission Line Media

Perhaps the most difficult RF performance specifications to meet are conversion loss and carrier suppression on the frequency translator and insertion loss on the linear modulator. Consequently, the circuit loss and the coupler directivity attainable are primary considerations in selecting suitable transmission line materials for the components. As mentioned in the introduction, alumina microstrip was satisfactory at low band, and the high band specifications make some allowance for increased loss and reduced coupler directivity in the high band. Therefore we expected that alumina microstrip would also be satisfactory in the high band. Nevertheless we felt it would be advisable to experiment with a couple of other alternatives in case we ran into trouble with the alumina microstrip.

In particular we chose to look at balanced stripline for the 3-dB hybrids, because we expected potentially lower loss and higher directivity by virtue of its wider line widths and uniform dielectric. For the diode arms of the modulator and the diode mounts in the translator mixers we considered Duroid microstrip because its loss should be comparable to alumina, the diode mounting would be convenient, and, if stripline couplers were used, the entire circuit could be printed on a single circuit board.

It is virtually impossible to decide among the various media with respect to loss on purely theoretical grounds, and one must resort to experimental comparisons. This fact is illustrated in Table 2.1, in which we compare the line losses at 10 GHz for alumina, and Duroid microstrip of different thicknesses, and for Duroid stripline, calculated from data or theory from several different sources. Note that the spread in calculated conductor losses for a given line greatly exceeds the differences among the lines, and that in general the losses of all the lines are roughly comparable. It is particularly important to note that although the conductor loss on microstrip increases as the thickness decreases, the radiation losses decrease and that the total loss is the same or lower for the thinner substrates. The radiation loss is calculated for open stub resonators. Neither the translator nor modulator have any such resonant elements, so the calculations probably greatly overestimate the radiation losses we would encounter.

TABLE 2.1 MICROSTRIP AND STRIPLINE LOSS COMPARISON
50 OHM LINE AT 10 GHz

| | Microstrip | | Stripline | |
|---|------------|---------|-----------|--------|
| | Alumina | Duroid | Duroid | |
| h - inch | 0.025 | 0.015 | 0.010 | 0.007 |
| h - cm | 0.064 | 0.038 | 0.025 | 0.018 |
| w/h | 0.95 | 0.95 | 3.0 | 3.0 |
| t/h | 0.008 | 0.013 | 0.14 | 0.20 |
| ϵ_r | 10.0 | 10.0 | 2.22 | 2.22 |
| ϵ_{eff} | 6.7 | 6.7 | 1.9 | 1.9 |
| λ_g - cm | 1.16 | 1.16 | 2.18 | 2.18 |
| $\tan \delta$ | 0.00005 | 0.00005 | 0.0008 | 0.0008 |
| Dielectric Loss, $\alpha_d \lambda_g$ (dB/wavelength) | | | | |
| | 0.0013 | 0.0013 | 0.018 | 0.018 |
| Conductor Loss, $\alpha_c \lambda_g$ | | | | |
| Schneider ^{1.} | 0.022 | 0.035 | 0.054 | 0.076 |
| PMH ^{2.} | 0.048 | 0.079 | 0.058 | 0.093 |
| BD ^{3.} | 0.053 | 0.090 | 0.098 | 0.132 |
| CHS ^{4.} | 0.039 | 0.167 | 0.130 | 0.180 |
| Howe ^{5.} | | | | 0.057 |
| MEH ^{6.} | | | | 0.114 |
| Radiation Loss, $\alpha_r \lambda_g$ | | | | |
| BD ^{3.} | 0.140 | 0.043 | 0.071 | 0.035 |
| Total Loss, $\alpha_t \lambda_g$ | | | | |
| BD ^{3.} | 0.194 | 0.134 | 0.187 | 0.087 |
| Howe ^{5.} | | | | 0.079 |

Ref.

1. M. V. Schneider, "Microstrip Lines for Microwave Integrated Circuits", BSTJ 48, pl421, May/June 1969.
2. R.A. Pucel, D. J. Masse, C.P. Hartwig, "Losses in Microstrip", MTT-16, p342, June 1968
3. E. Belohoubek, E. Denlinger, "Loss Considerations for Microstrip Resonators", MTT-23, p522, June 1975.
4. M. Caulton, J. Hughes, H. Sobel, "Measurements on the Properties of Microstrip Transmission Lines for Microwave Integrated Circuits", RCA Review 27, p377, Sept. 1966.
5. H. Howe, "Stripline Circuit Design", pl7, Artech House 1974.
6. Microwave Engineer's Handbook, Vol I, pl18, Artech House, 1971

2.2 3-dB Hybrids

The first trial couplers were a microstrip coupler on 0.020" alumina and a stripline coupler with 0.128" ground plane spacing. The microstrip coupler was a tandem connection of two 8.34 dB couplers, just as used on the low band circuits. We used a 0.020" substrate in an effort to keep the loss down. The stripline coupler was a single 3-section coupler using a 0.005" Duroid spacer between the overlapped, coupled lines. To obtain the desired 1.7 dB coupling for the center section with a 0.005" spacer we need a 0.128" ground plane spacing at the center section. To simplify the construction of the first trial coupler we carried this 0.128" ground plane spacing throughout the three sections and the feed lines, and hoped that higher order modes would not be excited.

Figures 2.2.1 and 2.2.2 show the test results on these initial couplers, after tuning them up for the best performance.

The microstrip coupler is somewhat over coupled, to about 2.6 dB, and there appears to be a lossy region just above the center frequency. The isolation, while falling short of the desired 25 dB, is still quite reasonable--better than 19 dB except at the extreme high end of the band, where it rolls off to about 14 dB. The VSWR is under 1.7 over the entire band. Aside from the high loss region, the insertion loss is roughly 1.1 to 1.4 dB, including the connectors, which contribute approximately 0.3 to 0.6 dB. Thus the coupler loss should be approximately 0.8 dB.

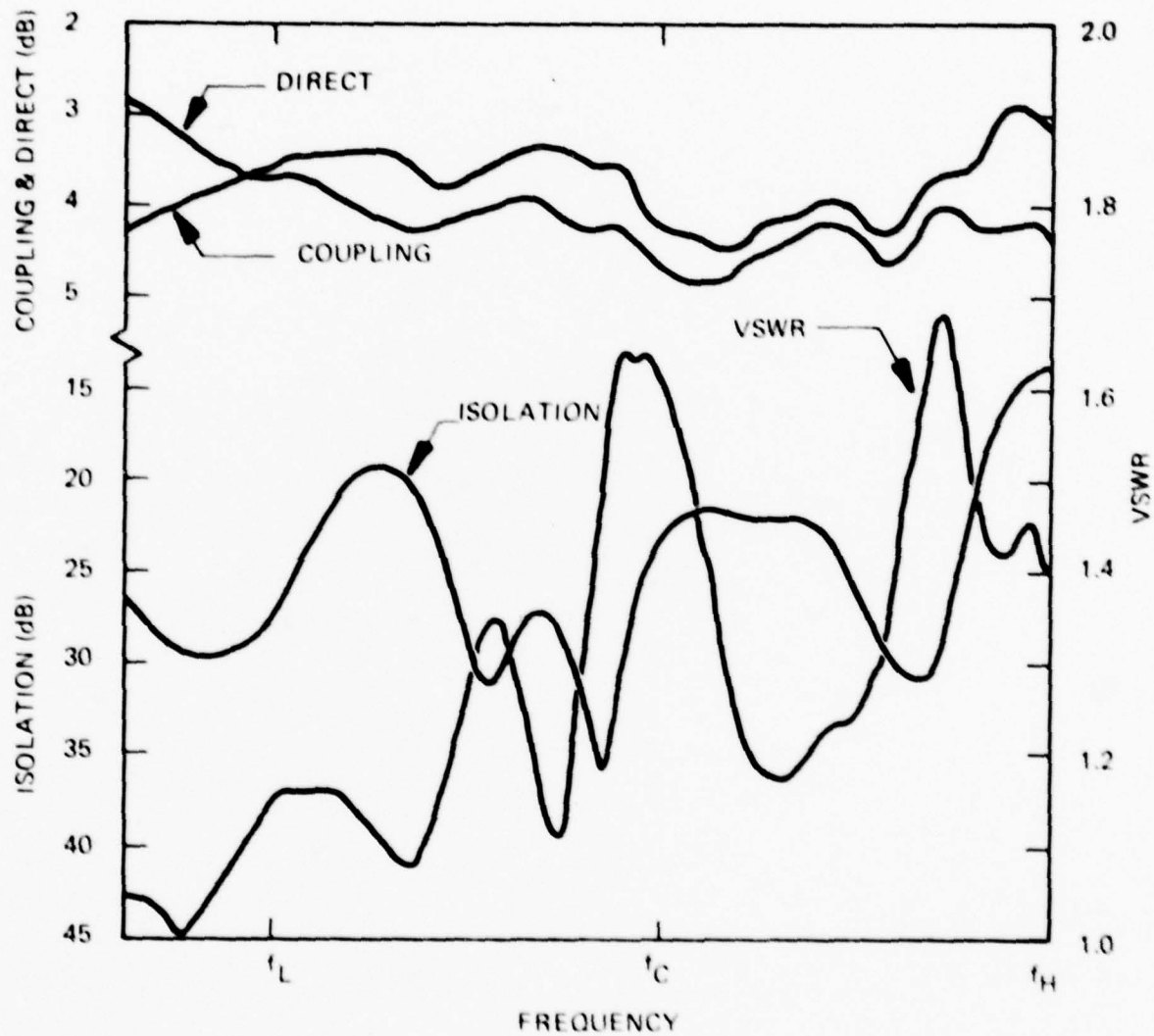


FIGURE 2.2.1 MEASURED RESPONSES OF 3 SECTION, TANDEM 8.34 dB MICROSTRIP 3-dB HYBRID ON .020" ALUMINA

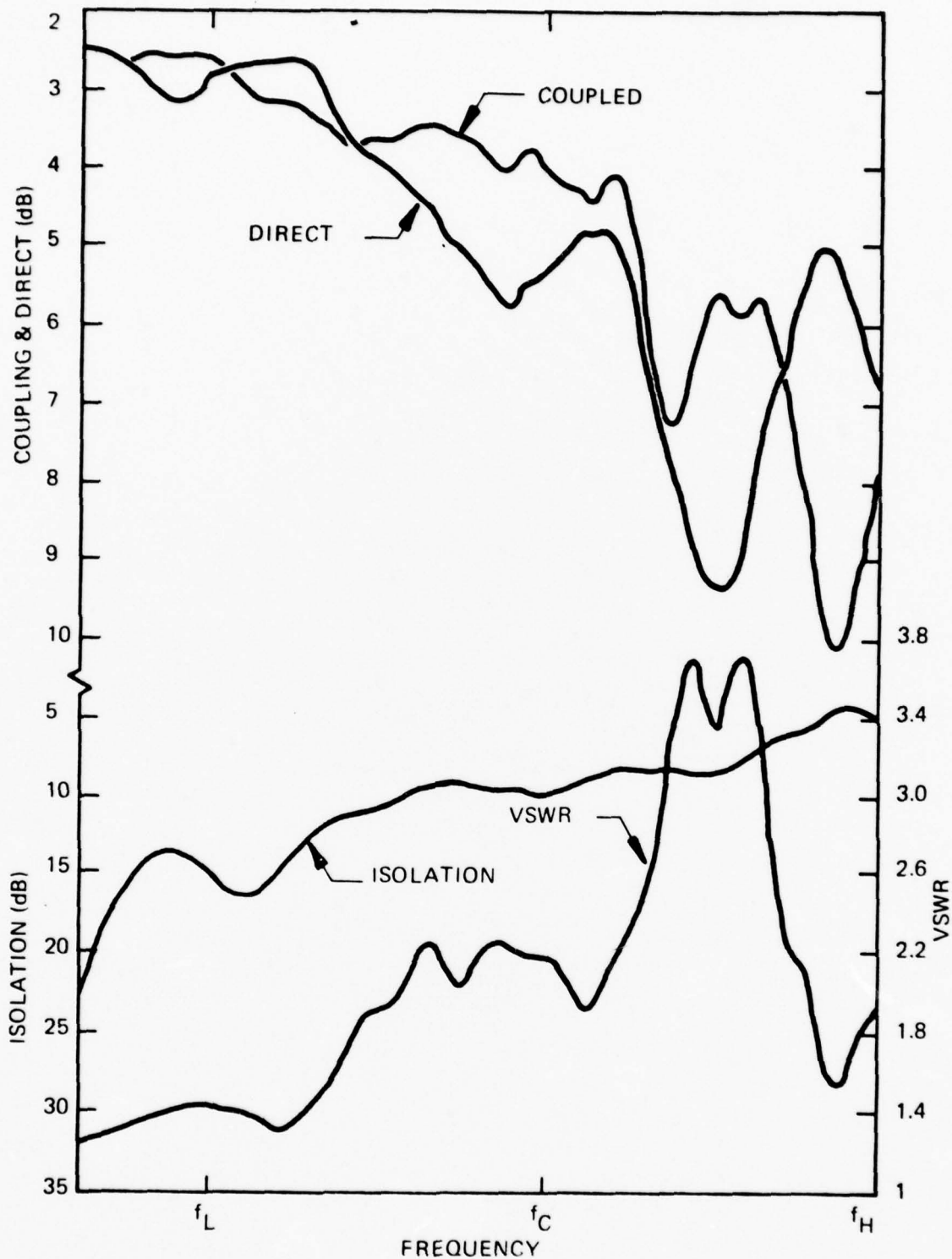


FIGURE 2.2.2 MEASURED RESPONSES OF 3-SECTION 3-dB STRIPLINE COUPLER WITH .128" GROUND PLANE SPACING

The stripline coupler did suffer higher order mode excitation in the upper half of the band, so that the response there is very unsatisfactory. In the vicinity of the lower band edge, it is reasonably close to a 3-dB coupler with a VSWR under 0.8 and loss of about 1 dB, with connectors. However, the isolation, above f_L , is never better than 16 dB, which was not very promising.

Another stripline coupler was made using a 1-mil teflon tape spacer between the lines in the center section, thereby reducing the ground plane spacing to 0.065". The results on this coupler are shown in Figure 2.2.3. Clearly, the higher order modes are absent and the coupler is well-behaved over the entire band. In particular, the loss runs from 0.5 to 1.1 dB, with connectors, and the mismatch is under 1.8. However, the isolation is still under 20 dB over substantial portions of the band.

We concluded then, that, although the insertion loss of the stripline coupler was lower than that of the microstrip coupler by 0.3 to 0.5 dB, the directivity of the stripline coupler was unsatisfactory, and that we were unlikely to achieve sufficient improvement by additional tuning. Therefore, we turned our attention to the alumina microstrip coupler which appeared to need only slight adjustments to the coupling and impedance levels, i.e. line widths and gaps. It should be remarked that connector mismatches contributed significantly to the low isolation near f_H on the microstrip coupler, and much effort was devoted to improving the connector match in the subsequent work.

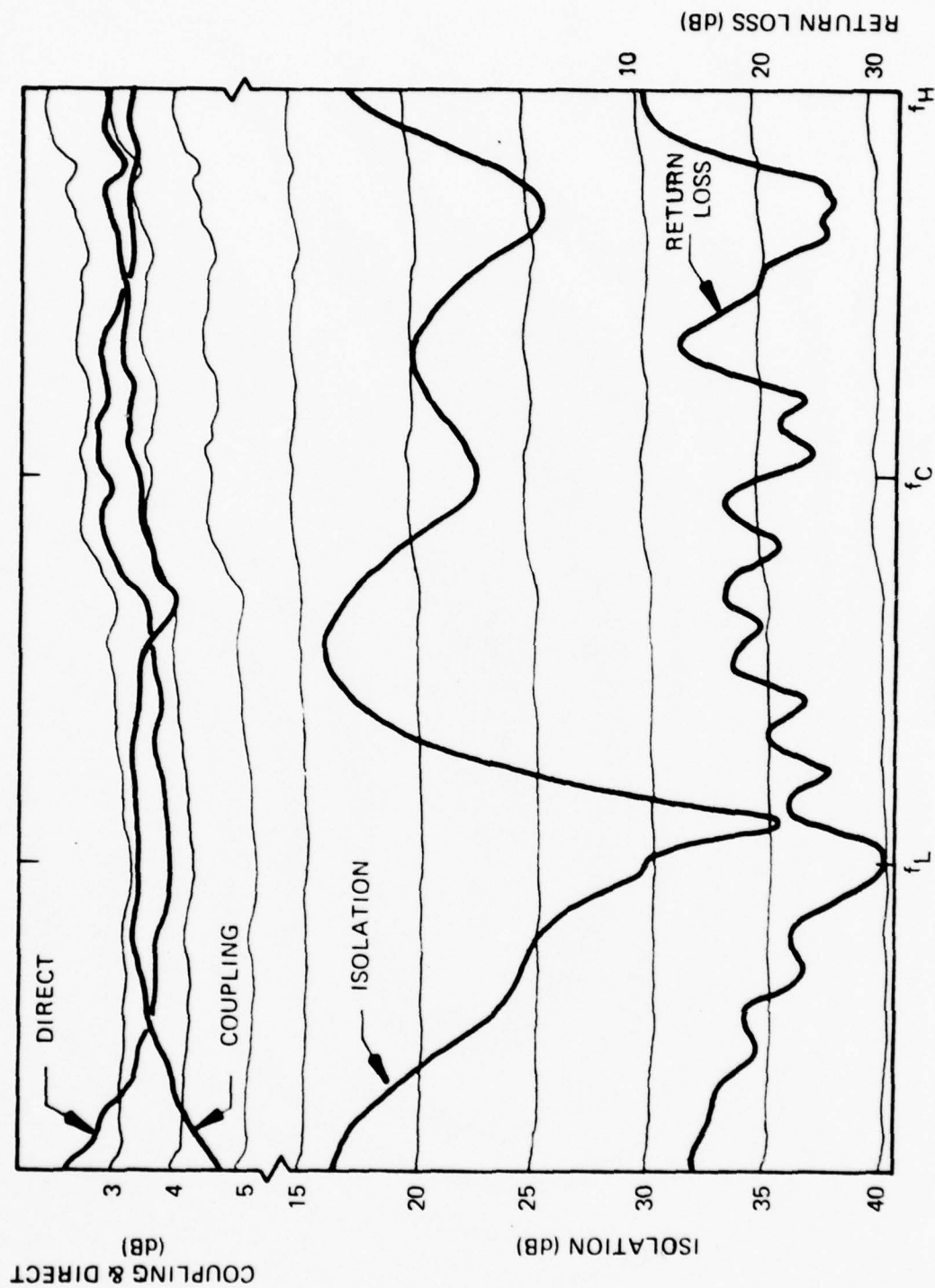


FIGURE 2.2.3 MEASURED RESPONSES OF 3-SECTION 3-dB STRIPLINE COUPLER WITH .065" GROUND PLANE SPACING.



The microstrip couplers on 0.020" alumina did not respond favorably to minor adjustments in gap and line widths and line lengths. In studying the problem we made and tested a series of 3-section 8.34 dB and single-section 6 and 22.7 dB couplers. The trend that emerged from these experiments was that the coupling was tighter and the center frequency about 25 percent higher than the design values, and that dielectric overlays did not consistently improve the directivity. Empirical corrections based on the single-section coupler data, resulted in 8.34 dB couplers that were still overcoupled and had reduced bandwidth. On reviewing all of that data, we noted that the measured coupling at the design center frequencies tended to be close to the design values. It appeared that the continued tightening of coupling at frequencies above the design center is a spurious effect, for which we have no ready explanation, and can only attribute to "higher order modes".

Since the usual cure for "higher order modes" in microstrip is a thinner substrate, we redesigned the coupler for 0.015" alumina. The results, following one simple correction, in which the center coupler was shortened and the ends lengthened by 5° , to flatten out the coupling slope, are shown in Figure 2.2.4. The coupling is quite flat across the band, ranging from 3.0 to 3.2 dB. The insertion loss runs from 1.1 to about 1.8 dB, including connectors, which is slightly higher than that on the 0.020" substrate. The isolation is better than 20 dB and the VSWR under 1.8 over the entire band; aside from the sharp roll off at f_H , they are better than 22 dB and 1.4 respectively. Also, it is very possible that the roll off is largely due to the connectors and adapters in the measuring system. In general, the performance is quite satisfactory except perhaps for the loss at the high end.

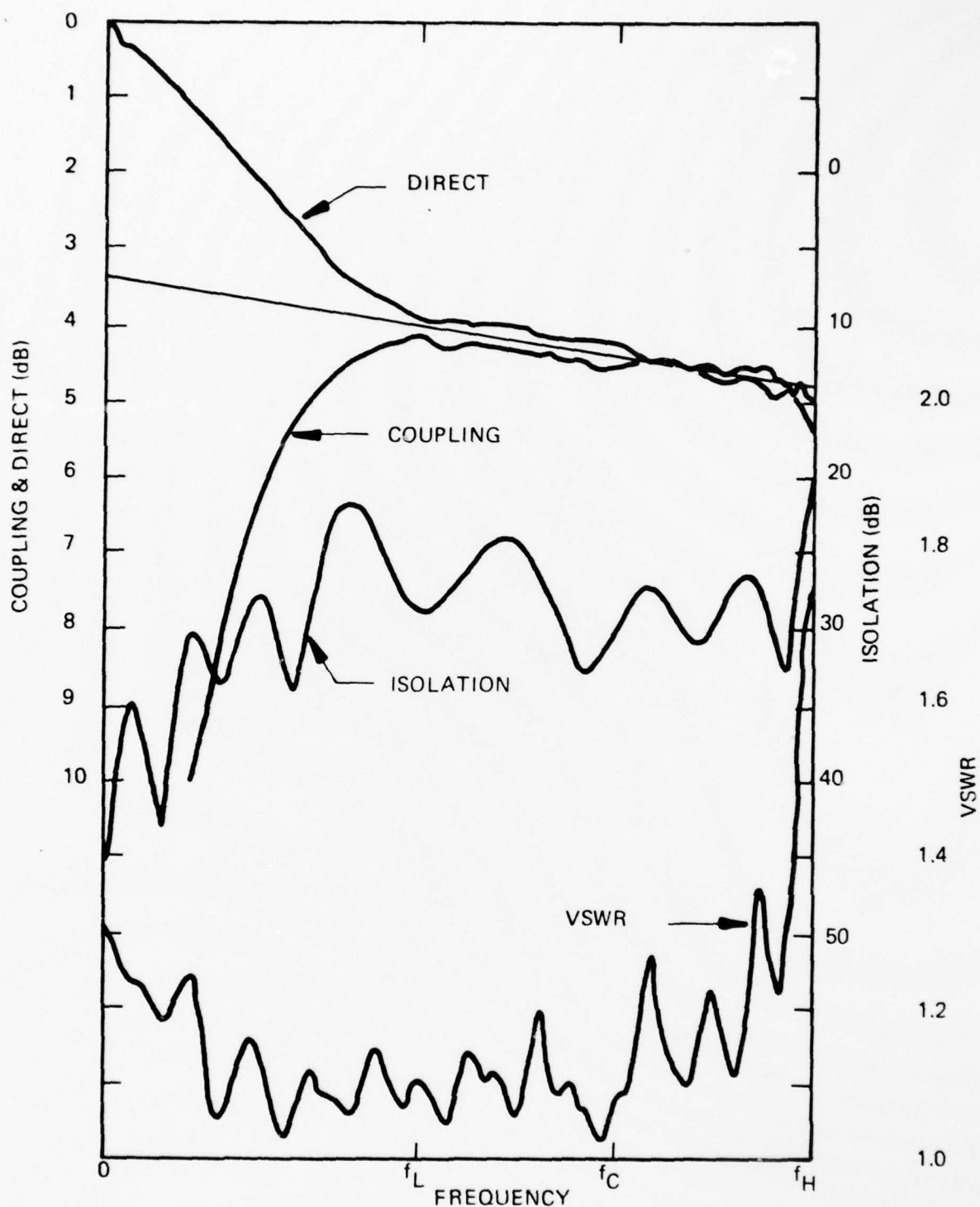


FIGURE 2.2.4 MEASURED RESPONSES OF 3-SECTION, TANDEM 8.34 dB, MICROSTRIP 3-dB HYBRID ON .015" ALUMINA

2.3 In-Phase Power Dividers

The first trial 3-section Wilkinson power dividers were on 0.020" alumina microstrip and Duroid stripline with 0.067" ground plane spacing. The resistors on both units were metalized alumina chip resistors.

The characteristics of the microstrip circuit are shown in Figure 2.3.1. The power split is excellent and the loss runs from approximately 0.3 to 0.8 dB. (There is an anomalous bump near f_H , which must be a measurement error, since it implies net gain.) The isolation is better than 17 dB, and the VSWR is under 1.8 both of which are quite acceptable for our application.

Suspecting that the VSWR and isolation peaks might be due, at least in part, by the excess capacitance of the alumina resistor chips, we made a divider on which the film resistors were made by leaving the chrome on the circuit board in the appropriate places. The results for this divider are shown in Figure 2.3.2. The improvement in isolation and VSWR was only slight, and the power split remained excellent. The insertion loss appears to have increased to 0.5 to 1.3 dB. However since the calibration level for the insertion loss measurement in Figure 2.3.1 is suspect, we believe that the loss in both cases is about the same and that the data in Figure 2.3.2 is reliable.

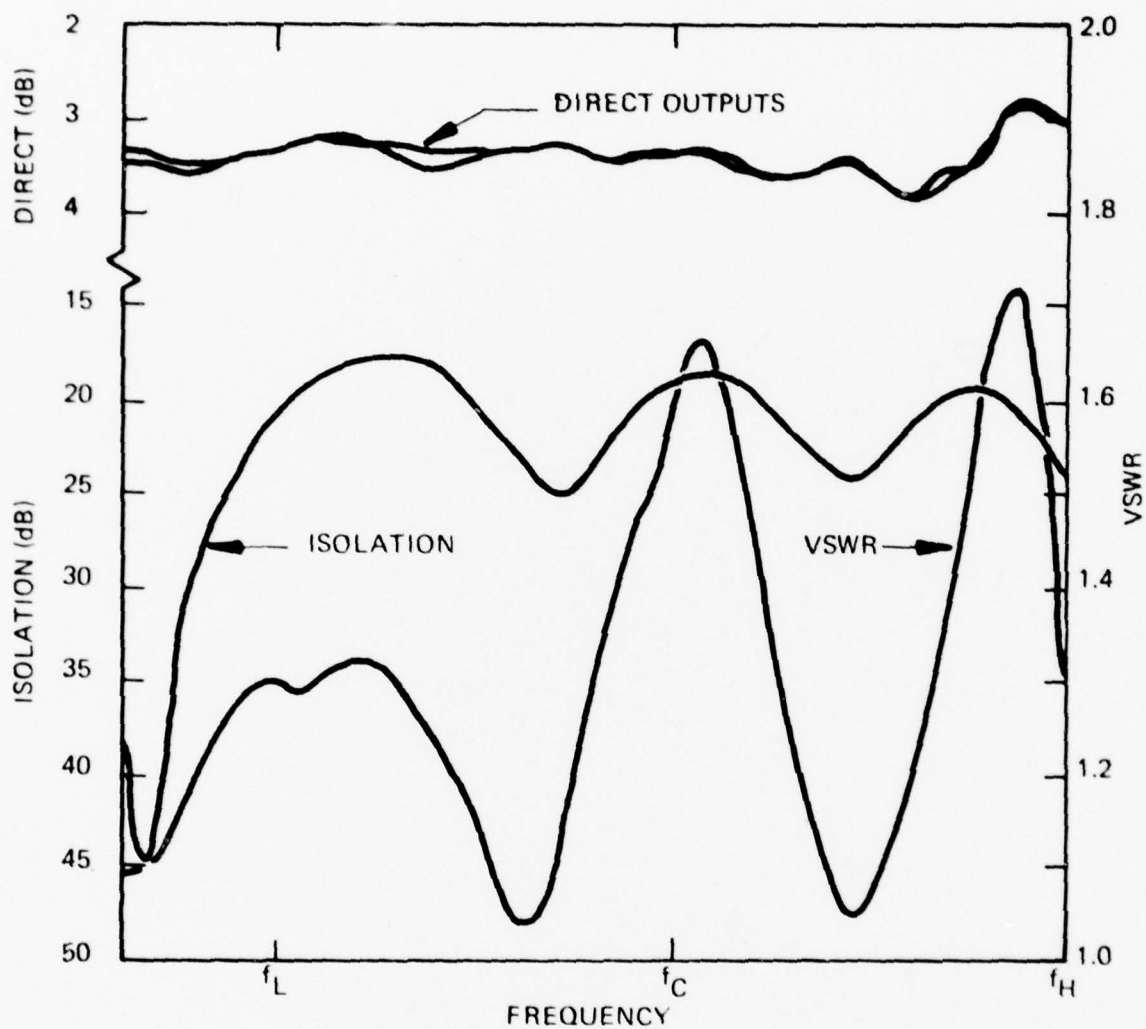


FIGURE 2.3.1 RESPONSES OF MICROSTRIP IN-PHASE POWER DIVIDER WITH CHIP RESISTORS

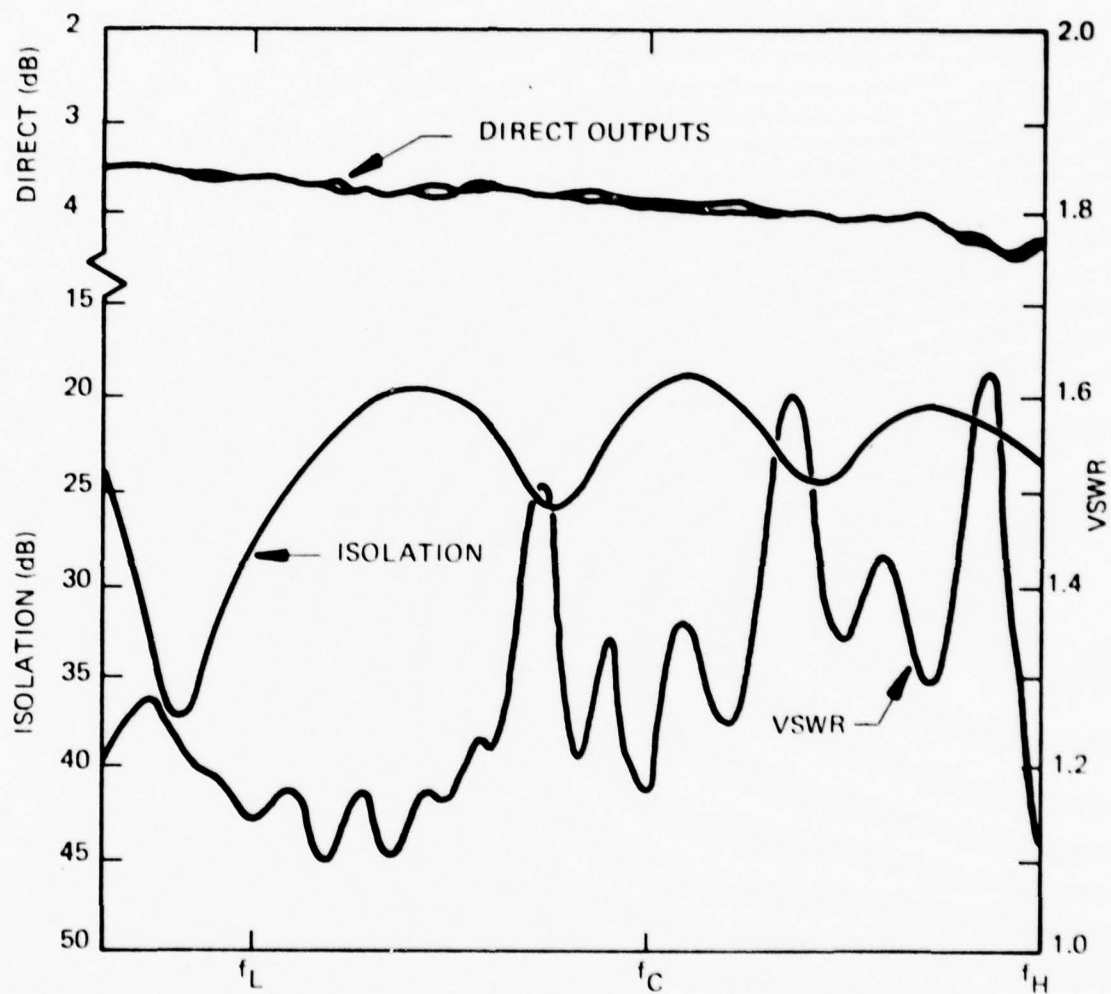


FIGURE 2.3.2 RESPONSES OF MICROSTRIP IN-PHASE POWER DIVIDER WITH ETCHED RESISTORS

Figure 2.3.3 shows the responses of the stripline coupler. Since its performance is obviously unacceptable, and the microstrip coupler works so well, we made no further effort to make the stripline divider work.

Although we were forced to go to 0.015" alumina for the 3-dB hybrids, there appeared to be no evidence of higher order modes in the 20-mil power dividers. Therefore, in order to keep the loss down, we used 0.020" material for the divider and 0.015" material for the couplers in the frequency translator.

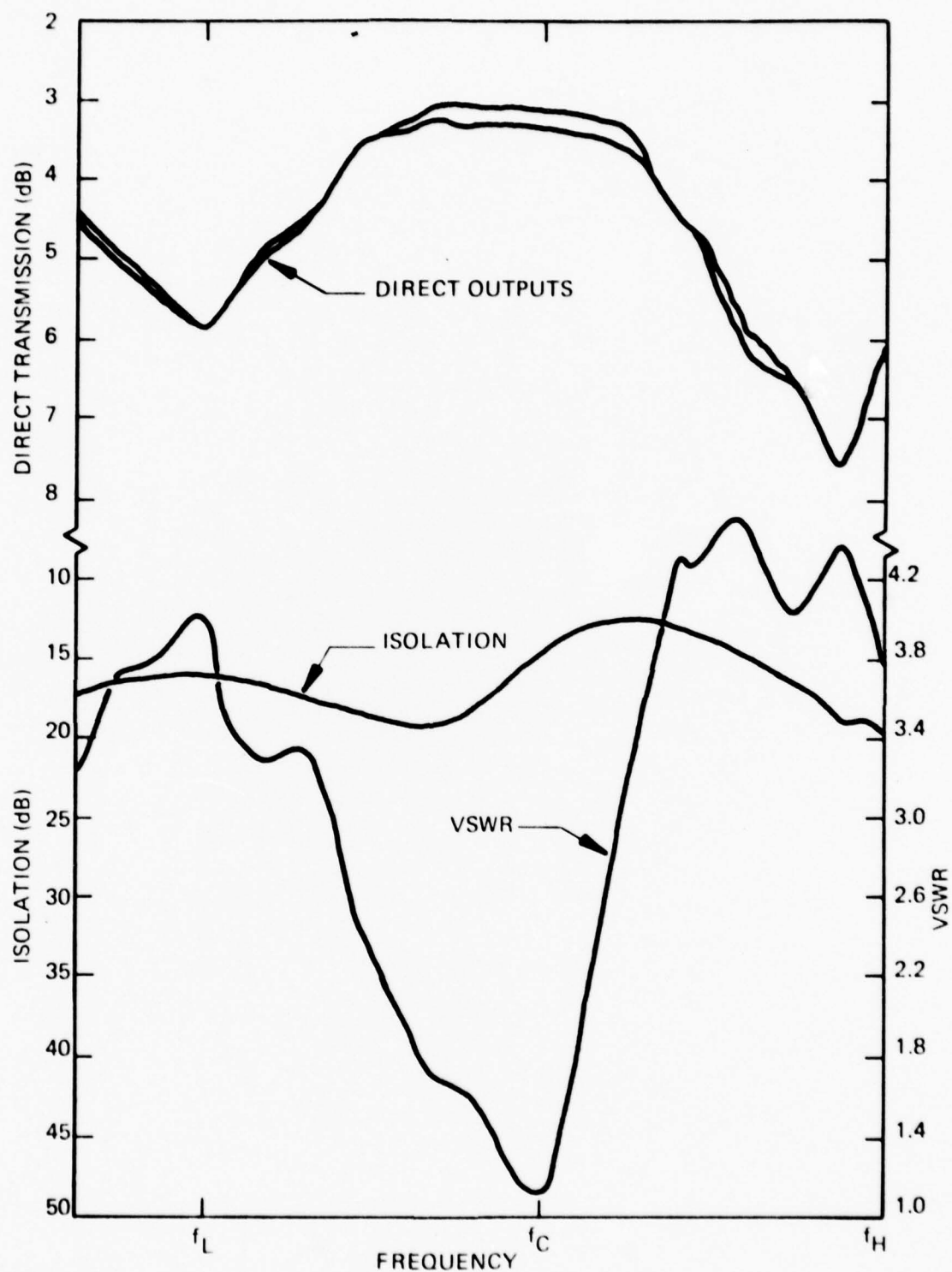


FIGURE 2.3.3 RESPONSES OF STRIPLINE IN-PHASE POWER DIVIDER

2.4 Bias Tee for Frequency Translator

On the frequency translator an excellent match to the mixer diodes is required at its quiescent operating point, i.e. in the absence of the baseband modulation. Therefore a broad band, well-matched bias network is required through which to apply the modulation.

The bias tee network used consists of a quarter-wave 100-ohm stub at the center of a half-wave 42.5 ohm matching section. The stub is terminated with a 20 pF chip bypass capacitor. Figure 2.4.1 shows the layout of a dual bias lead test circuit to check out the match and loss of a bias tee and the RF cross-talk between leads. The dotted line indicates the portion of this circuit used for tuning the network with a diode in place.

The loss, VSWR and isolation between leads are given in Figure 2.4.2. The large VSWR spike near f_H is due to connector-adaptor mismatches, which were a constant problem in this frequency range. The behavior of the bias tee itself is excellent, and it required no further tuning to obtain the desired broadband diode match.

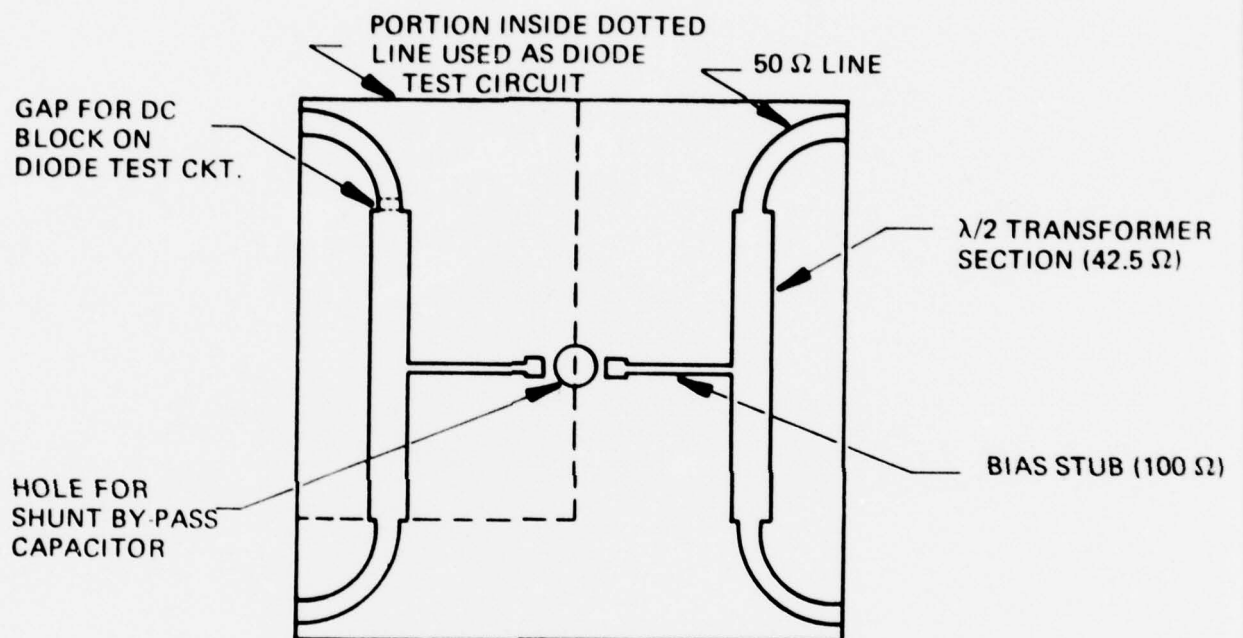


FIGURE 2.4.1 DUAL BIAS LEAD TEST CIRCUIT

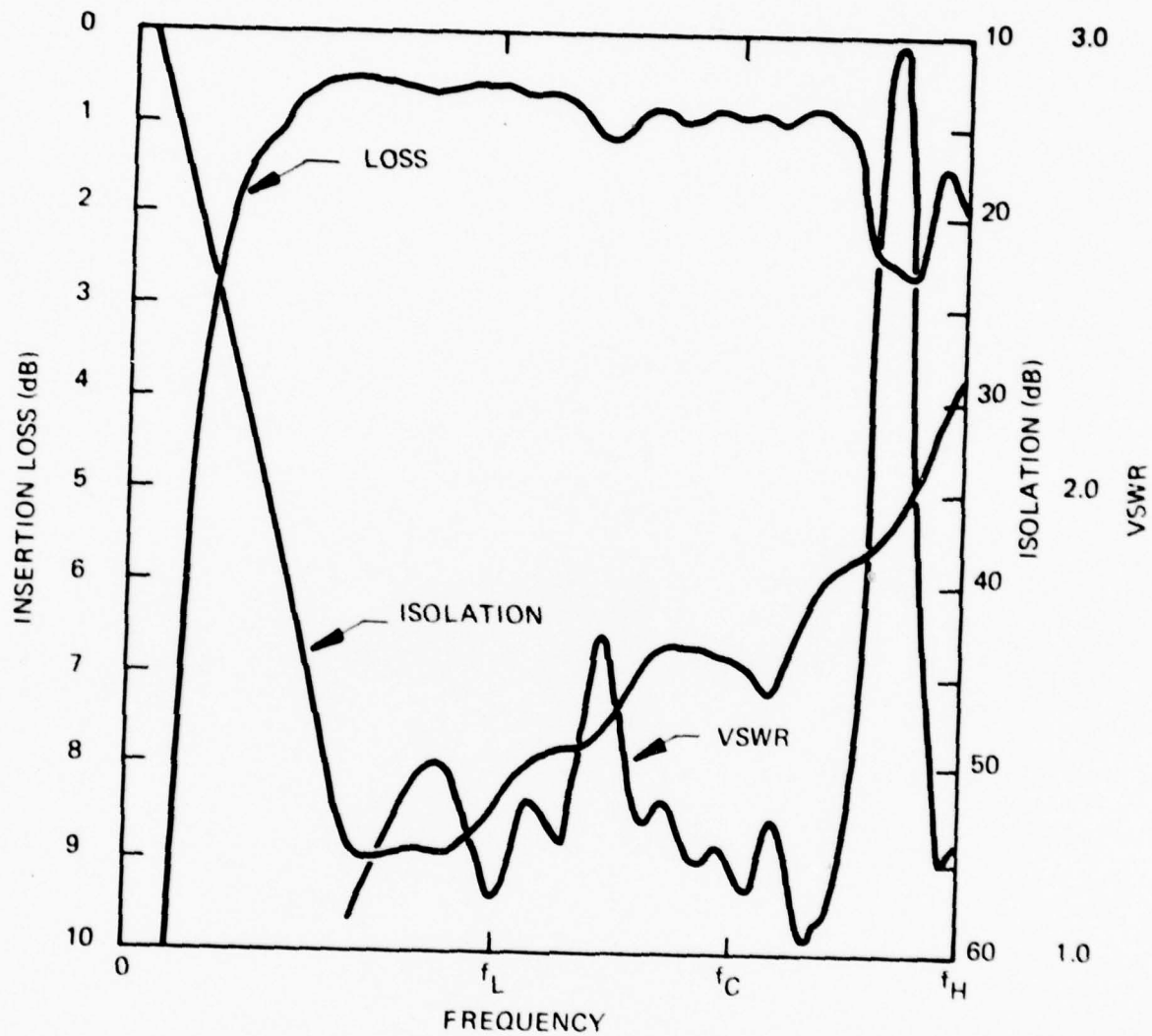


FIGURE 2.4.2 CHARACTERISTICS OF DUAL BIAS LEAD TEST CIRCUIT

2.5 Frequency Translator Baseband Modulator

The theory and design of the baseband modulator was covered in detail in the final reports for the two low band contracts. Since the high band translator used the same modulator as the second low band unit, and no further development was undertaken, we will not report the whole story here. Instead, we will simply summarize its basic design features.

The baseband modulator section, shown in block form in Figure 1.2.2 consists of an input driver, a pair of phase shifting networks, a sideband selector switch, and a pair of output voltage drivers. The input driver splits the audio input signal at the desired offset frequency into two outputs equal in amplitude and 180° out of phase which drive the phase shifter networks. The latter are all-pass RC filters designed for an output phase difference of $90^\circ \pm 2^\circ$ over the entire base band. The selector switch transfers the audio frequency drive between diodes for upper and lower sideband generation. The output voltage drivers provide a low source impedance and the dc bias for the modulator diodes in the RF section.

The input driver in the baseband modulator, shown schematically in Figure 2.5.1, provides a low-impedance, balanced input to the phase shifting networks. Both phase and amplitude balance are essential to accurate phase shift. The ac-coupled input signal passes through a unity gain emitter follower to provide the " + " output, while the " - " output is derived from an inverting operational amplifier connected in the feed-forward mode. This circuit maintains accurate phase and amplitude balance over the base band from -55°C to $+110^\circ\text{C}$.

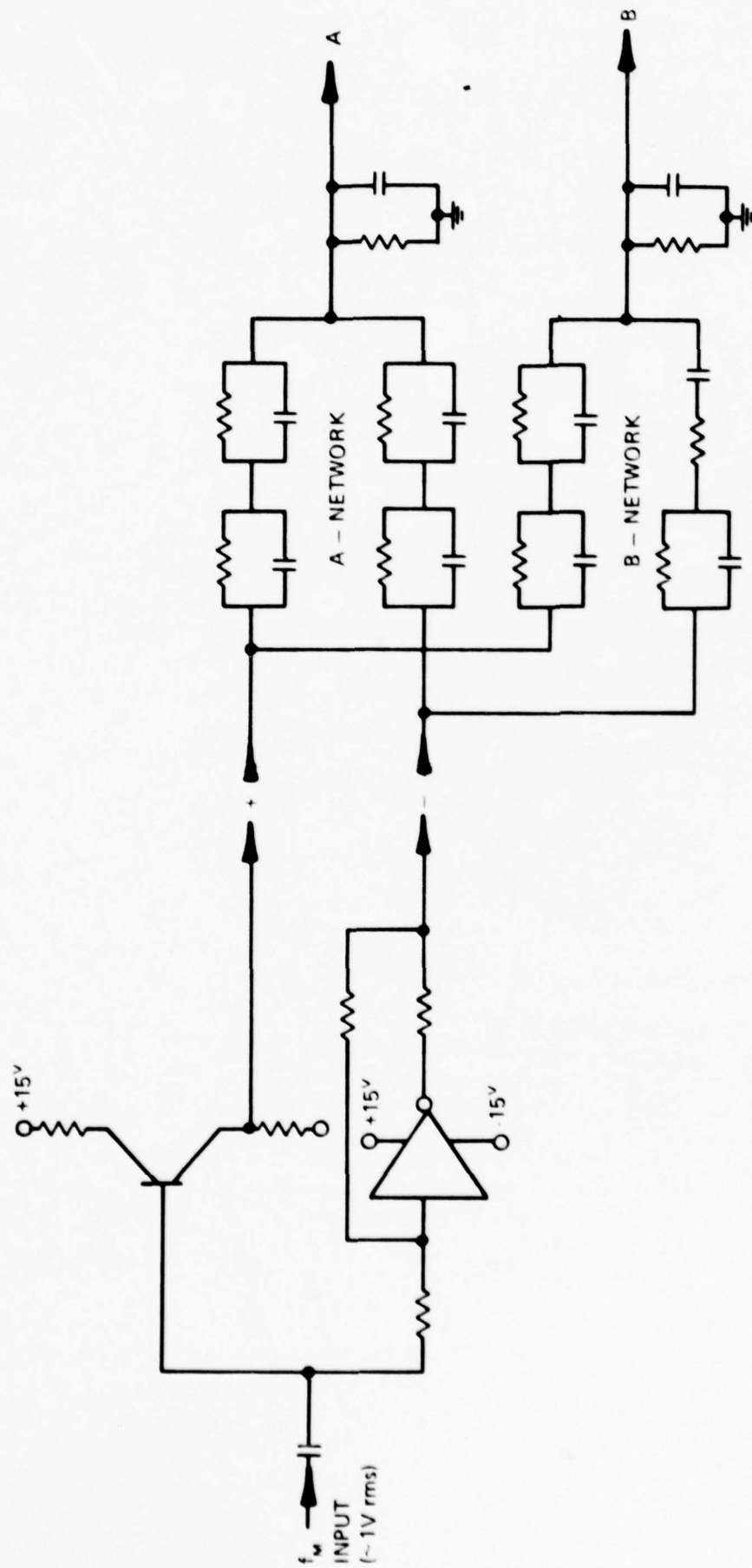


FIGURE 2.5.1 BASEBAND MODULATOR INPUT DRIVER AND RC PHASE SHIFT NETWORK TOPOLOGY

The key element of the baseband modulator is the phase difference network which provides a quadrature phase difference between the outputs while maintaining amplitude balance over a 1000:1 bandwidth. It consists of two all-pass RC phase shifting filters, shown schematically in Figure 2.5.1 designed to maintain a 90° difference with a $\pm 2^\circ$ ripple over the 3 decades. The design is based on the synthesis procedure developed by Weaver^{*}. The phase error is 0 to $+4.5^\circ$ and the voltage imbalance is less than 5 percent over the 1000:1 bandwidth.

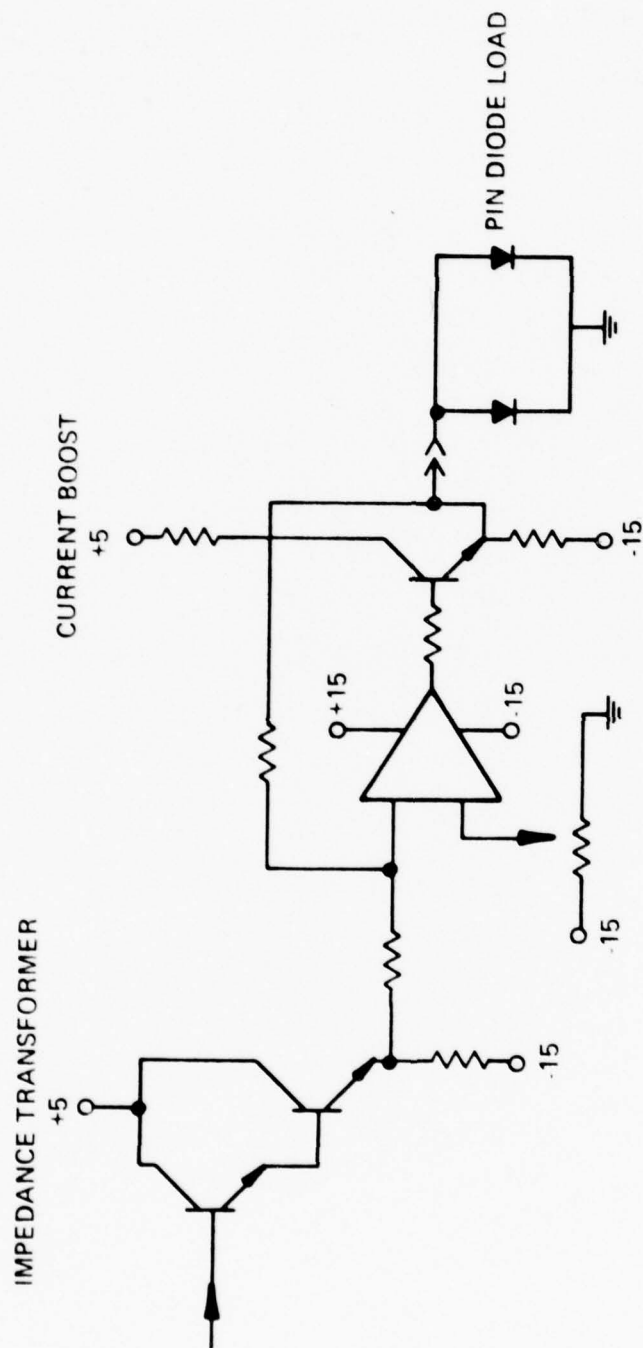
The sideband selector switch is an integrated circuit dual SPDT switch using CMOS FET's as the active switching elements.

The output voltage driver, Figure 2.5.2, consists of an impedance transformer, an amplifier section, and a current boost transistor. The transformer provides a high impedance termination to the phase shift network and a low impedance source to the amplifier. The amplifier recovers the signal attenuation in the phase shifter, and the current boost provides a low source impedance to the diode load.

2.6 Linear Modulator Driver

The modulator driver is the same as that used on the second low-band linear modulator. Its design and operation are described in detail in the final reports for the two low band contracts, and will not be repeated here. The complete schematic diagram is given in Figure 2.6.1 for reference.

* D. K. Weaver, "Design of a Wide-Band 90° Phase Difference Network," Proc. IRE 42, pp671-676, April 1954



DC BIAS ADJUST
(TEMPERATURE COMPENSATED)

FIGURE 2.5.2 BASEBAND MODULATOR OUTPUT DRIVER (ONE SIDE)

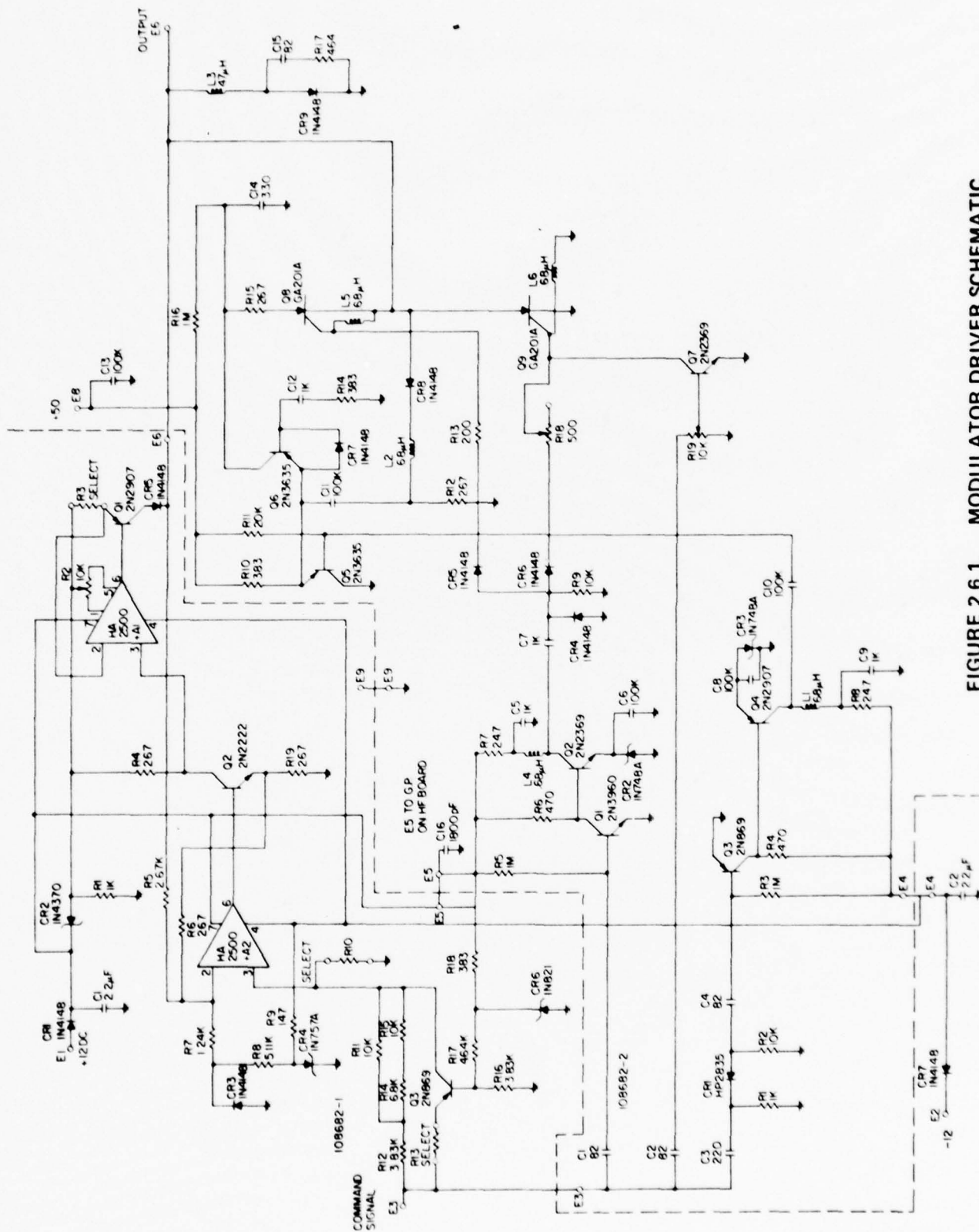


FIGURE 2.6.1. MODULATOR DRIVER SCHEMATIC

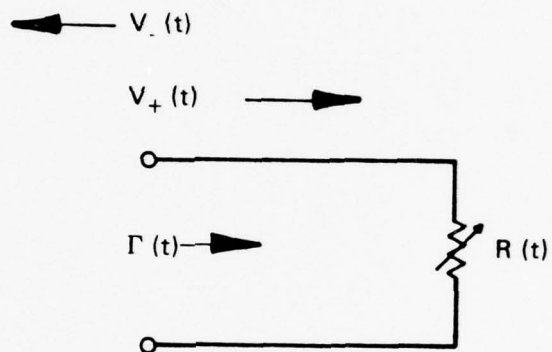
3. FREQUENCY TRANSLATOR

3.1 Theory

The RF section of the translator is an image cancelling single-sideband modulator, as shown schematically in Figure 1.2.1. The input carrier is split by a broadband in-phase power divider and fed to the two quadrature hybrid coupled mixers. The baseband modulation is applied to the two mixers in phase quadrature. The phases of the upper and lower sidebands coming from each mixer are such that they are separated by the output hybrid as shown. If the phase of the modulation applied to the lower terminal is changed from -90° to $+90^{\circ}$, the sideband outputs are reversed.

Ideally, the impedance of the mixer diodes should be purely resistive, and the resistance should vary such that the reflection coefficient varies sinusoidally at the modulation frequency as identified in Figure 3.1.1. When this condition is met only the desired first order, and no higher order, sidebands are generated. Furthermore, if the time average of the reflection coefficient is zero, the carrier is completely suppressed. Note that the minimum conversion loss for each sideband is 6 dB which occurs for 100 percent modulation.

Forward biased PIN diodes come close to satisfying these ideal requirements. First, they have very little parasitic reactance, making them essentially voltage or current variable resistors so that a broadband match can be readily obtained at a fixed bias level. Second,



$$\begin{aligned}
 V_-(t) &= V_+(t) \Gamma(t) \\
 &= V_0 \cos \omega_0 t [\Gamma_0 + \Gamma_1 \cos \omega_m t] \\
 &= V_0 \Gamma_0 \cos \omega_0 t + \frac{V_0 \Gamma_1}{2} [\cos (\omega_0 + \omega_m) t + \cos (\omega_0 - \omega_m) t]
 \end{aligned}$$

CARRIER SUPPRESSED WHEN $\Gamma_0 = 0$

MINIMUM CONVERSION LOSS IS 6 dB WHEN $\Gamma_1 = 1$

FIGURE 3.1.1 IDEAL RESISTIVE MIXER SIDEBAND GENERATOR

the reflection coefficient as a function of bias voltage varies anti-symmetrically about the match. Figure 3.1.2 shows the reflection coefficient characteristic for a PIN diode chip termination a 50 ohm microstrip line. The solid line is a 5th order polynomial fit to the data over the range shown. Although the reflection coefficient does not vary linearly with the applied voltage, the polynomial contains only odd powers of the voltage excursion from the match up to $\Gamma = \pm 0.8$. Consequently, if the diode is driven sinusoidally at the modulation frequency by a voltage source, only odd order sidebands will be generated. Figure 3.1.3 shows the conversion loss and ratio of third to first order sideband levels as a function of the ac drive amplitude calculated for the polynomial shown in Figure 3.1.2. Note that for drive levels in the 0.12 to 0.17 volt range, the conversion loss is less than 9 dB and the 3rd order suppression is better than 15 dB. Although some waveshaping circuitry could be employed in the driver to reduce the amplitudes of the higher harmonics, these results indicate that such complexity is not required.

Figure 3.1.4 summarizes how the translator performance depends on the performance of the individual components. It is important to note that the carrier suppression is governed by the directivity of the mixer quadrature hybrid couplers as well as each diode match. Also the rejection of the unwanted (image) sideband requires phase and amplitude balance between the two mixers.

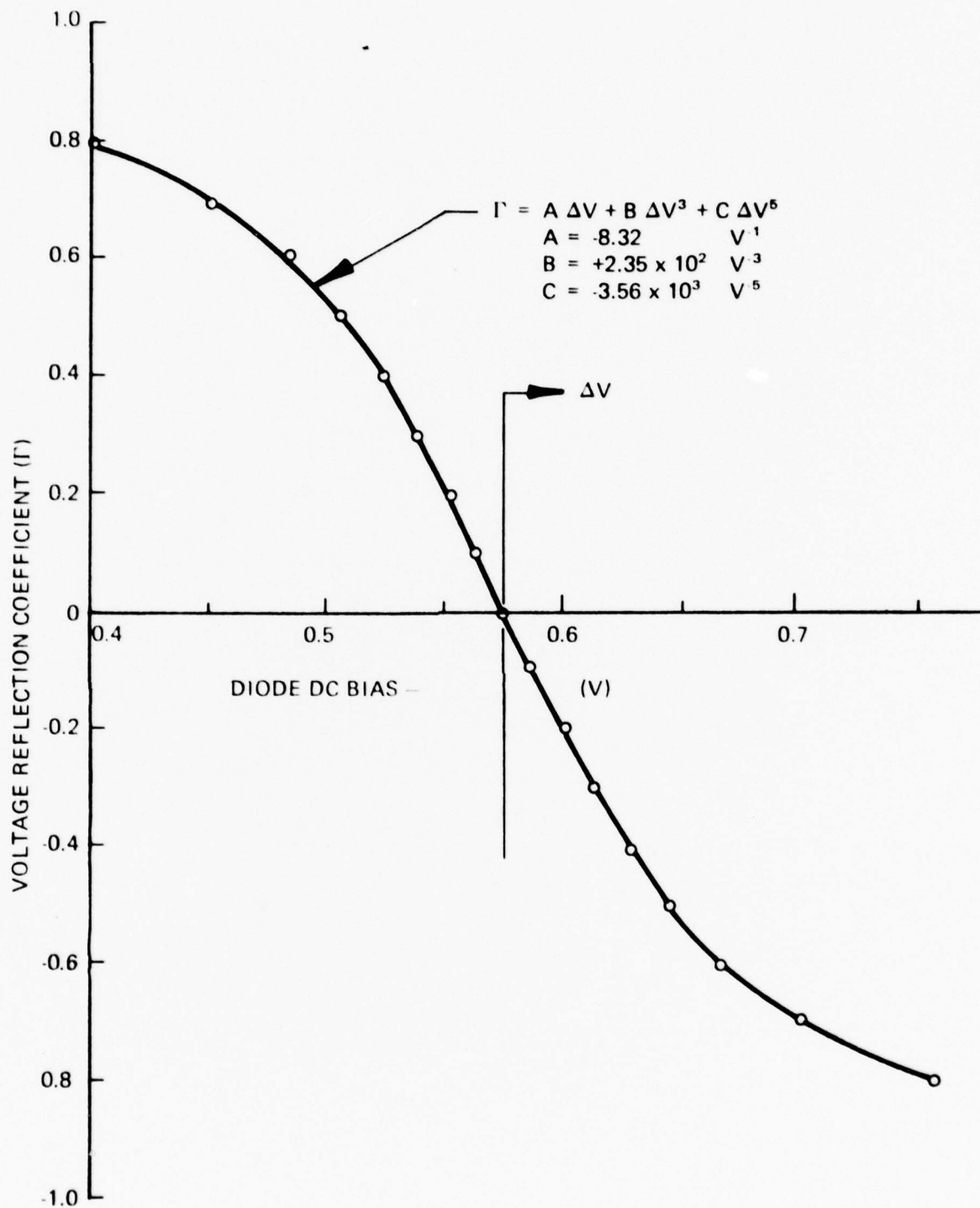


FIGURE 3.1.2 PIN MODULATOR DIODE REFLECTION COEFFICIENT VS. DC BIAS VOLTAGE

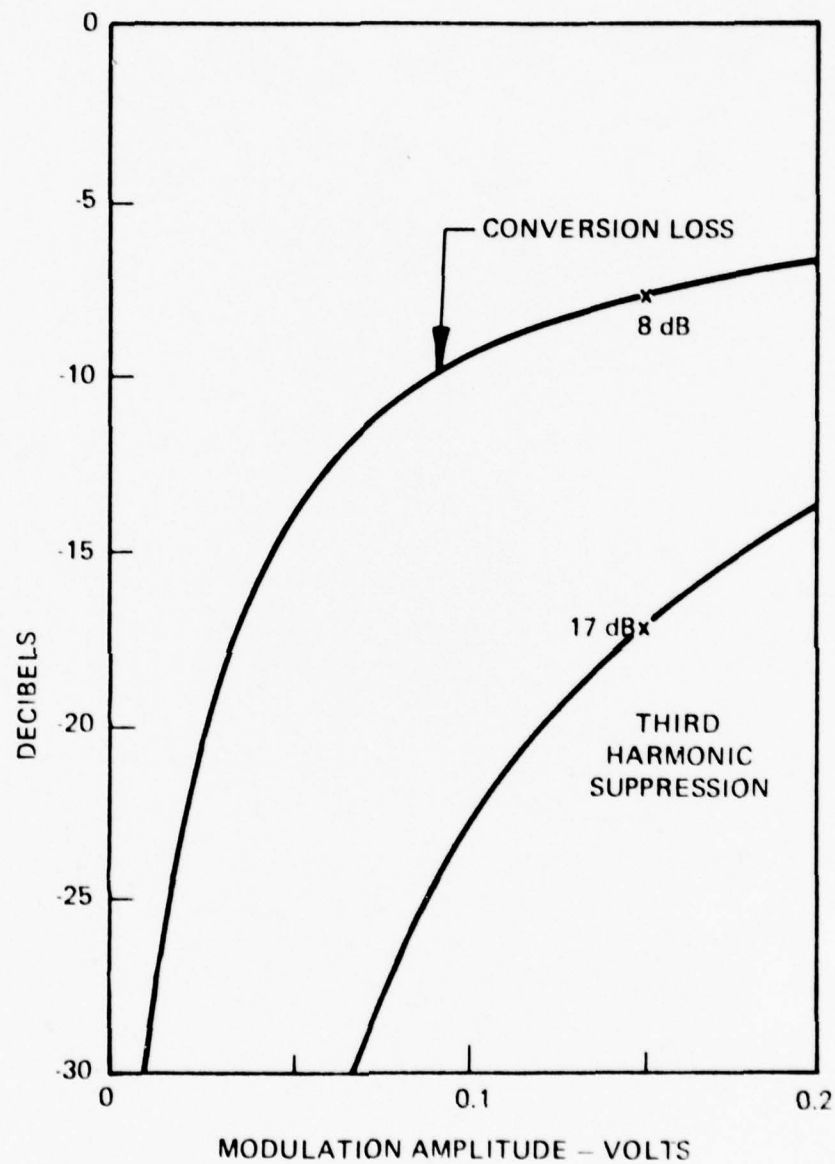


FIGURE 3.1.3 CALCULATED CONVERSION LOSS & THIRD HARMONIC SUPPRESSION VS. PIN DIODE AC DRIVE LEVEL

| PERFORMANCE FACTOR | CONTROLLING CIRCUIT FACTORS |
|-----------------------------|--|
| CONVERSION LOSS | RF CIRCUIT LOSS MODULATION AMPLITUDE |
| CARRIER SUPPRESSION | 3 dB HYBRID DIRECTIVITY DIODE MATCH AT ZERO DRIVE |
| IMAGE REJECTION | INPUT POWER SPLIT 3 dB HYBRID COUPLING BALANCE MODULATION PHASE QUADRATURE MODULATION AMPLITUDE BALANCE |
| SPURIOUS SIDEBAND REJECTION | DIODE R V RELATIONSHIP DIODE REACTANCE MODULATION VOLTAGE WAVEFORM |
| RF POWER LIMIT | DIODE NON-LINEARITY AT HIGH RF LEVELS |

FIGURE 3.1.4 RELATIONSHIP OF TRANSLATOR PERFORMANCE TO CIRCUIT CHARACTERISTICS

3.2 Layout and Construction

The layout of the mixer circuit board is shown in Figure 3.2.1, and Figure 3.2.2 is a photograph of the RF section. Refer to Figure 1.2.1 for the schematic diagram of the network. The input power is equally split by a 3-section Wilkinson power divider and then fed to two balanced mixers, each consisting of a 3-dB 90° hybrid coupler with its direct and coupled arms terminated with PIN diodes. The outputs of the mixers, from the fourth arms of the hybrids are fed to another 3-dB 90° hybrid such that the upper and lower sidebands emerge from the two output ports, as indicated in Figure 1.2.1.

This power divider is on .020" thick, 99.5 percent pure alumina microstrip, and the load resistors are etched from the chrome base layer of the Cr-Au-Cu-Au metalization. In the corner of the power divider substrate, a chrome square with two gold contacts can be seen. This was used to check the metalization resistances. The initial resistance was approximately 80-90 ohms per square. This was trimmed up to 100-110 ohm per square by quickly etching the chrome in dilute etchant.

Each 3-dB hybrid consists of a tandem pair of symmetrical 3-section 8.34 dB couplers with dielectric overlays to improve the directivity. The overlays are of 3-M Epsilam-10 material, cemented down with a TiO_2 - loaded styrene glue. The mixer substrates also have the bias tee networks, the PIN diodes and MOS dc blocking capacitors. The latter are visible in the photo adjacent to the input and output substrates. Metalized alumina chip capacitors are mounted on the circuit floor, through holes in the mixer substrates, to serve as RF bypass capacitors.

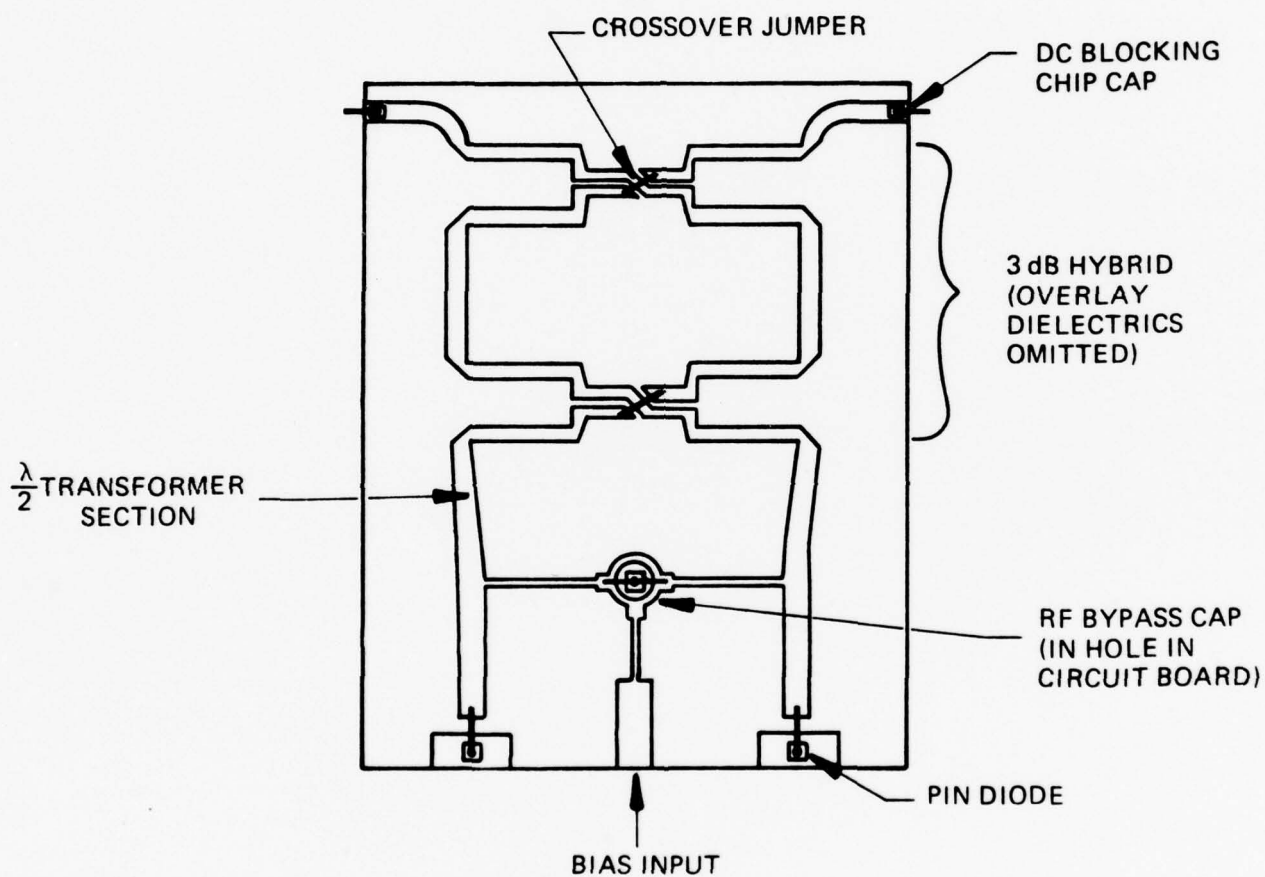


FIGURE 3.2.1 FREQUENCY TRANSLATOR MIXER CIRCUIT LAYOUT

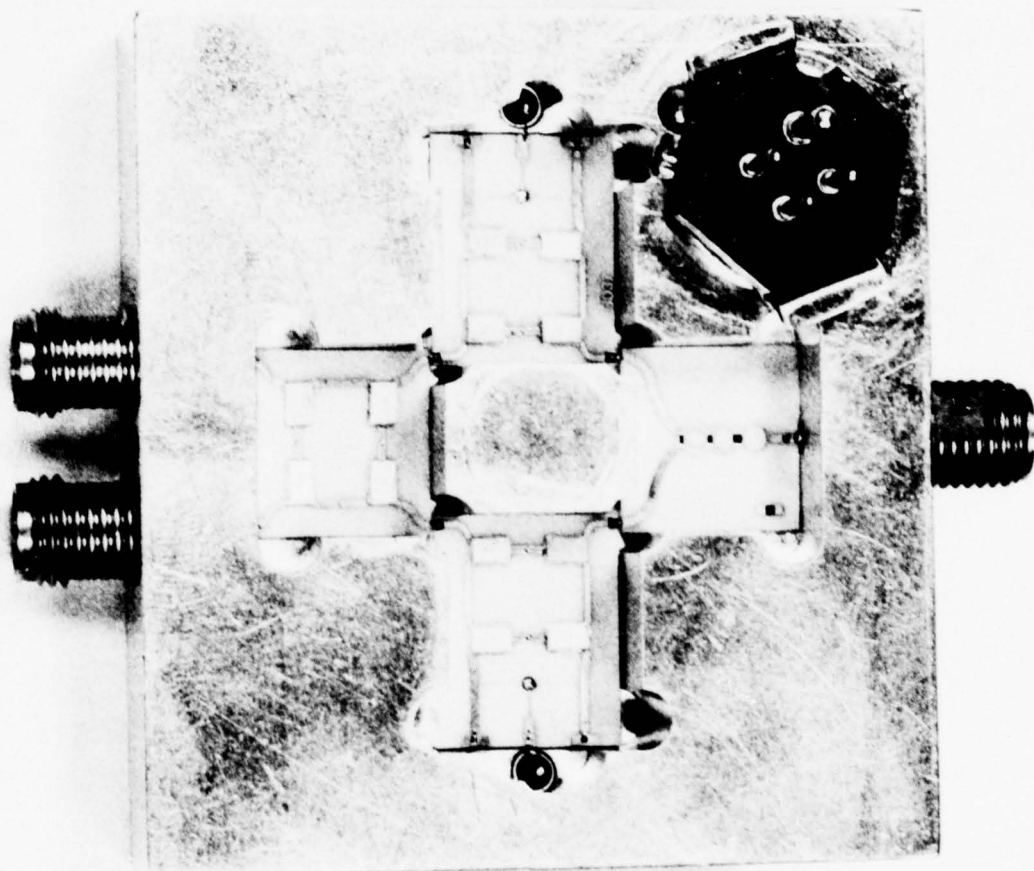


FIGURE 3.2.2 HIGH BAND FREQUENCY TRANSLATOR

The ac drive, from the baseband modulator, is applied via the 4-prong plug and the glass-metal feedthroughs clearly visible in the photo.

3.3 Performance Data

Typical performance data for the complete translator--RF and baseband modulator sections--are plotted in Figures 3.3.1 and 3.3.2. The data were taken for a fixed offset frequency and input power level, but the results are essentially independent of offset frequency over the baseband bandwidth and input power up to at least 100 mW. The conversion loss data for the desired side band are relative to the input power at the in-phase power divider. Carrier, undesired side band, and 3rd order side band suppression levels are relative to the desired sideband output level. All other spurious outputs are at least 10 dB below the 3rd order sideband.

The dc offset voltage to each diode was approximately 0.58V and the ac modulation amplitude on the diodes was about 0.2V. This implies, from Figure 3.1.3, a minimum theoretical conversion loss of 7 dB and 3rd order sideband suppression of 13 dB, which is in reasonable agreement with the data.

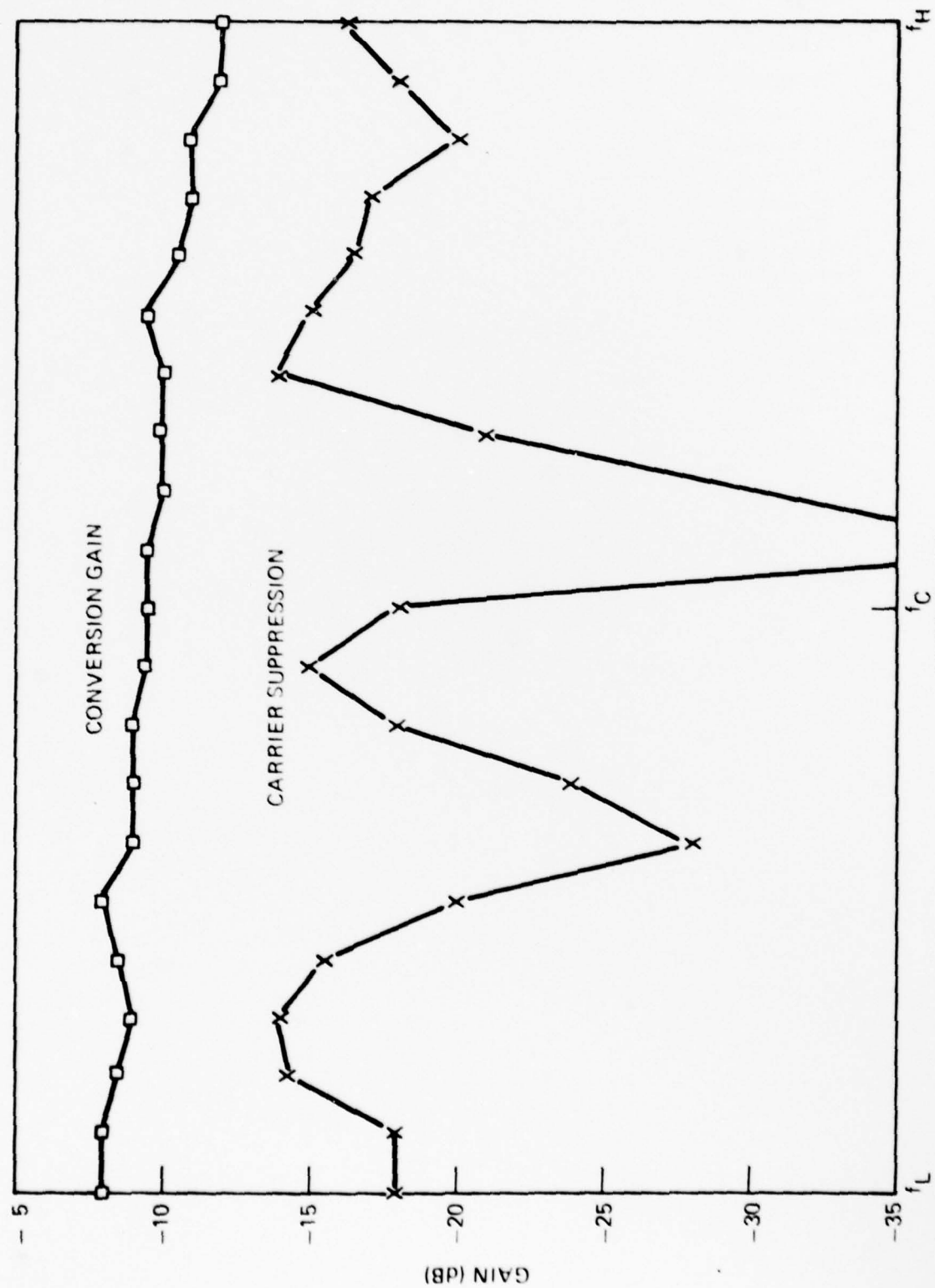


FIGURE 3.3.1 HIGH BAND FREQUENCY TRANSLATOR CONVERSION GAIN & CARRIER SUPPRESSION



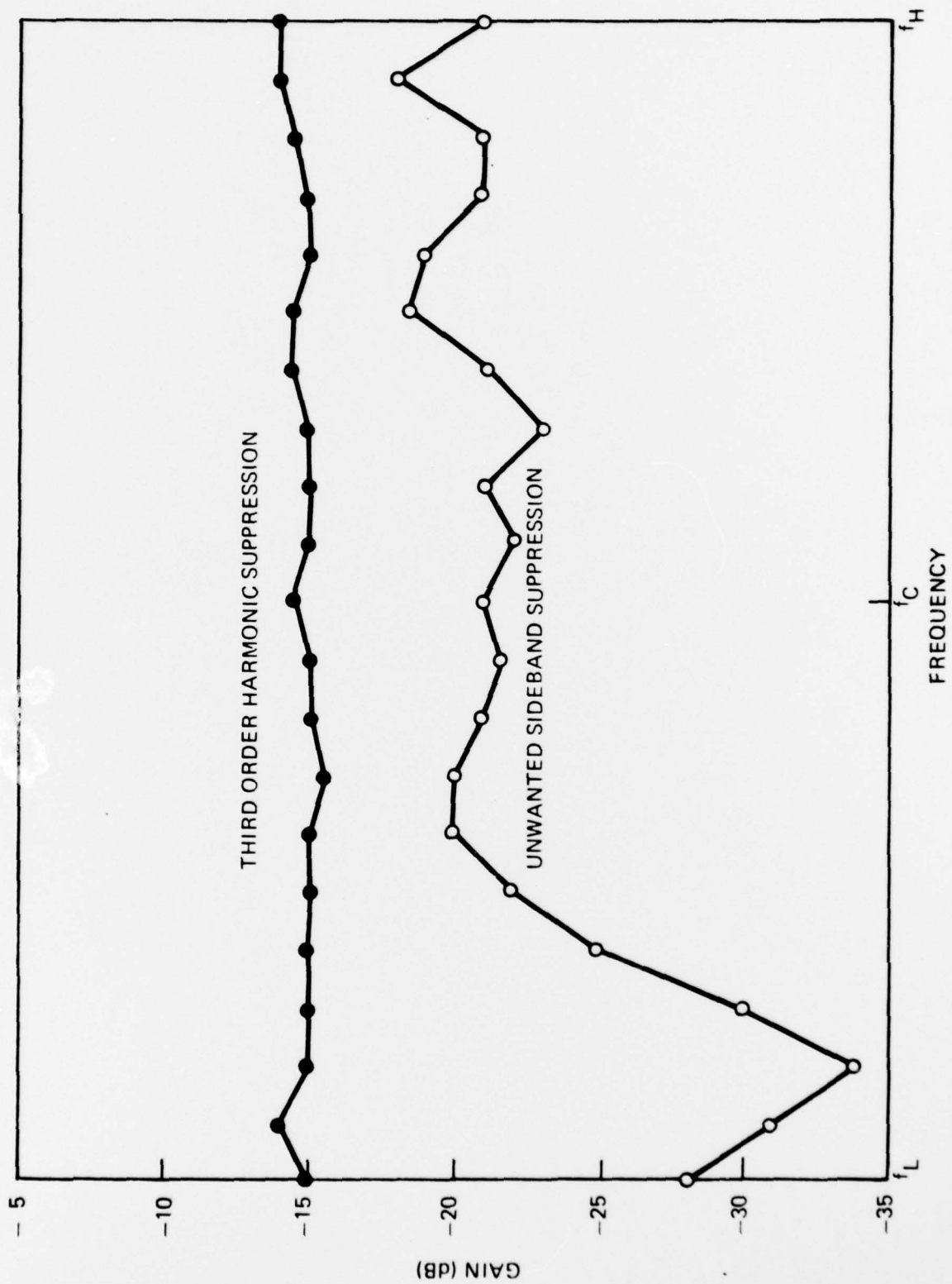


FIGURE 3.3.2 HIGH BAND FREQUENCY TRANSLATOR THIRD ORDER & UNWANTED FIRST ORDER SIDEBAND SUPPRESSION



The conversion loss increases fairly smoothly from 8 to 12 dB from f_L to f_H . Assuming a 7 dB theoretical conversion loss, the circuit insertion loss runs from approximately 1 to 5 dB. If we estimate the insertion loss to be expected on the basis of the data on the individual components, making allowance for the connector losses, we would expect it to run from about 1.8 to 3.8 dB. This estimate is admittedly very crude, but it does indicate that the complete translator is considerably lossier at the high end than the individual components would suggest. We were unable to determine the source of this excess loss on this program, but there appears to be room for at least a 1 dB improvement in the high end conversion loss, bringing it reasonably close to the 10 dB goal.

4. LINEAR AMPLITUDE MODULATOR

4.1 Design Considerations

As mentioned in the Introduction, the VSWR and bandwidth required led to the matched attenuator configuration of Figure 1.3.1, employing the same broadband 3-dB hybrids used in the frequency translator.

In the matched attenuator circuit, reflections from the two diode arms, assumed to be equal in amplitude and 90° out of phase, will combine in phase in the terminated port on the input end. Transmitted power, also equal in amplitude and 90° out of phase, will combine in phase in the output port. The terminated port at the output is isolated. The input match is governed primarily by the connector and coupler matches, and by the coupling balance. Coupler directivity is not critical here as it is in the translator.

Although series-mounted diodes are always more convenient in microstrip, the insertion loss is higher and the isolation per diode tends to be lower than can be attained with shunt-mounted diodes. Therefore, the latter are dictated for this application. For shunt-mounted diodes, the attenuation flatness is governed by the number of quarter-wavelength spaced diodes used--the more diodes, the less flat the attenuation versus frequency. The number of diodes is fixed by the maximum isolation attainable from each diode, which in turn is governed by the minimum diode resistance. In the modulator it was possible to get the 45 dB dynamic range with just two diodes in each arm, however to do so required driving the diodes so far into saturation that linearization would become a difficult problem. Consequently, three-diode arms were necessary. However, the insertion loss penalty was negligible, being less than 0.1 dB.

It would have been possible to use the same broadband, distributed bias lead in the modulator as was used in the translator. However, since its match in this application is not so critical, it was possible to use lumped element choke coils and bypass capacitors. This allowed us to keep the total line length short and the diode-arm channels very narrow.

The major problem area on the modulator is the tradeoff between power handling and switching speed. Fast switching requires a thin I-layer PIN diode which is susceptible to rectification at low attenuation levels. This results in the attenuation varying with input power level. To avoid this thick I-layer diodes must be used, which switch more slowly, with a given driver. In the low band development we concluded that a 2-mil I-region diode was the minimum acceptable with respect to power handling. Accordingly, a driver was developed to switch the 2-mil diodes from the low loss state to any higher attenuation in under 60 ns, including delay. Since the maximum input power level on the high band unit is less than on the low, it would be possible to use a thinner diode. However, since the 2-mil diode-driver combination had been developed together to work satisfactorily, we elected to keep this combination in the high band modulator.

4.2 Layout and Construction

Figure 4.2.1 is a photograph of the complete linear modulator, including driver. The RF section is mounted directly on top of the driver to keep the driver output leads as short as possible.

The 3-dB hybrids are on .015" alumina, and the diode arms are on .007" Duroid. The 10 pF MOS dc blocking capacitors are mounted on each end of the Duroid boards such that the top of the capacitor is almost even with the top of the alumina board. Then the bonding strap runs essentially straight across to the alumina board, with minimum inductance and serving also as the interboard connection.

The driver lead feeds up through to center of the RF housing via a glass-metal feedthrough and is wire-bonded to alumina chip bypass capacitors to each side. Small, several-turn choke coils, not quite discernable in the photo, are connected from the capacitors to the lines.

4.3 Performance Data

The attenuation versus frequency and VSWR data for several bias levels are given in Figures 4.3.1 and 4.3.2; the attenuation versus command voltage in Figure 4.3.2.

At zero bias, the insertion loss runs from 1.8 to 4.2 dB, f_L to f_H , or 3.0 ± 1.2 dB. This is not quite as flat as the desired ± 1.0 dB, and the high end loss exceeds the desired 3.5 dB maximum considerably. At the 10 dB level, 0.5 mA diode current, the variation is down to ± 0.9 dB, within the ± 1.0 or 10 percent specification. From the 20 to 50 dB levels the flatness is within 7 percent.

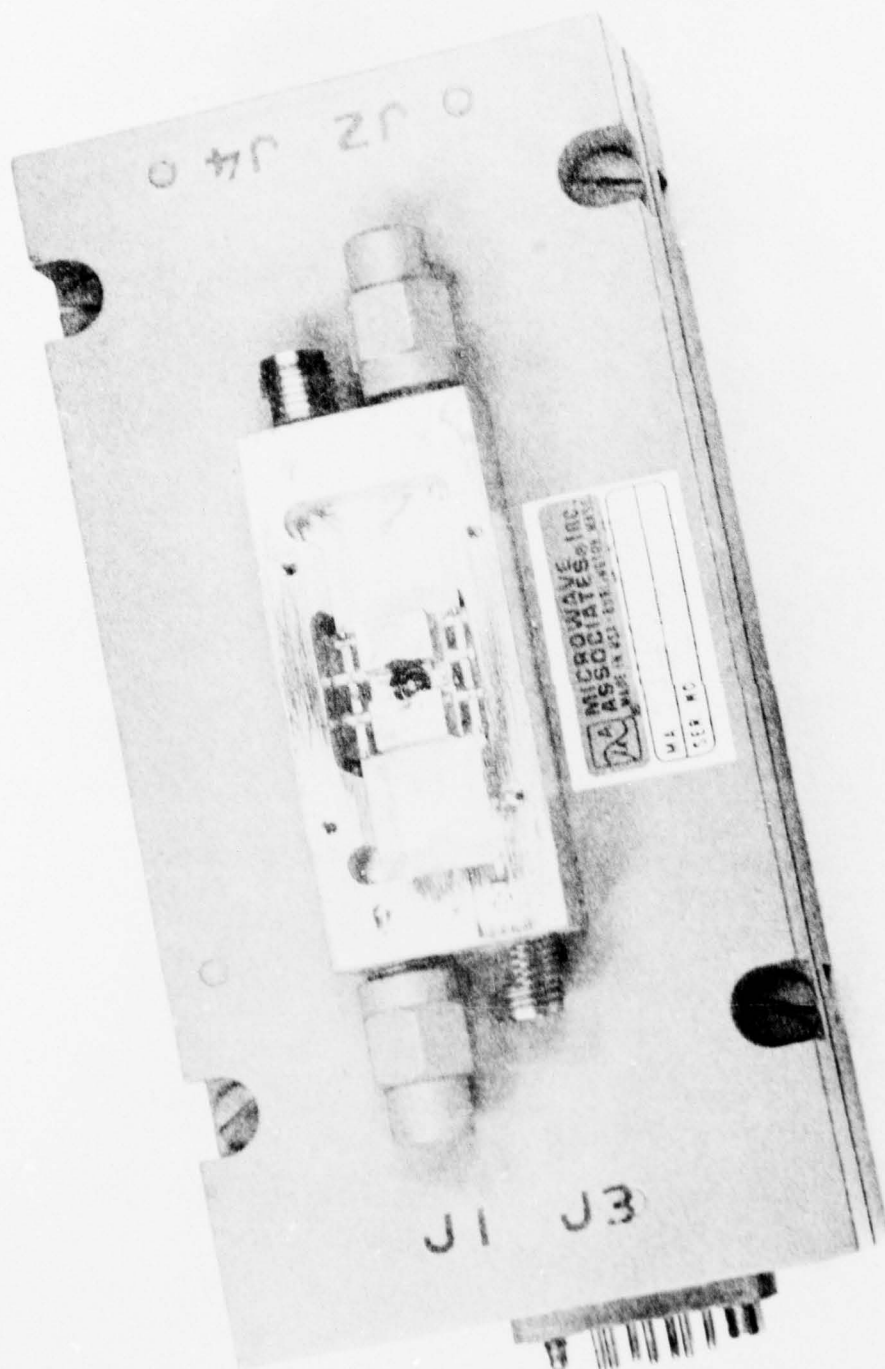


FIGURE 4.2.1 HIGH BAND LINEAR AMPLITUDE MODULATOR

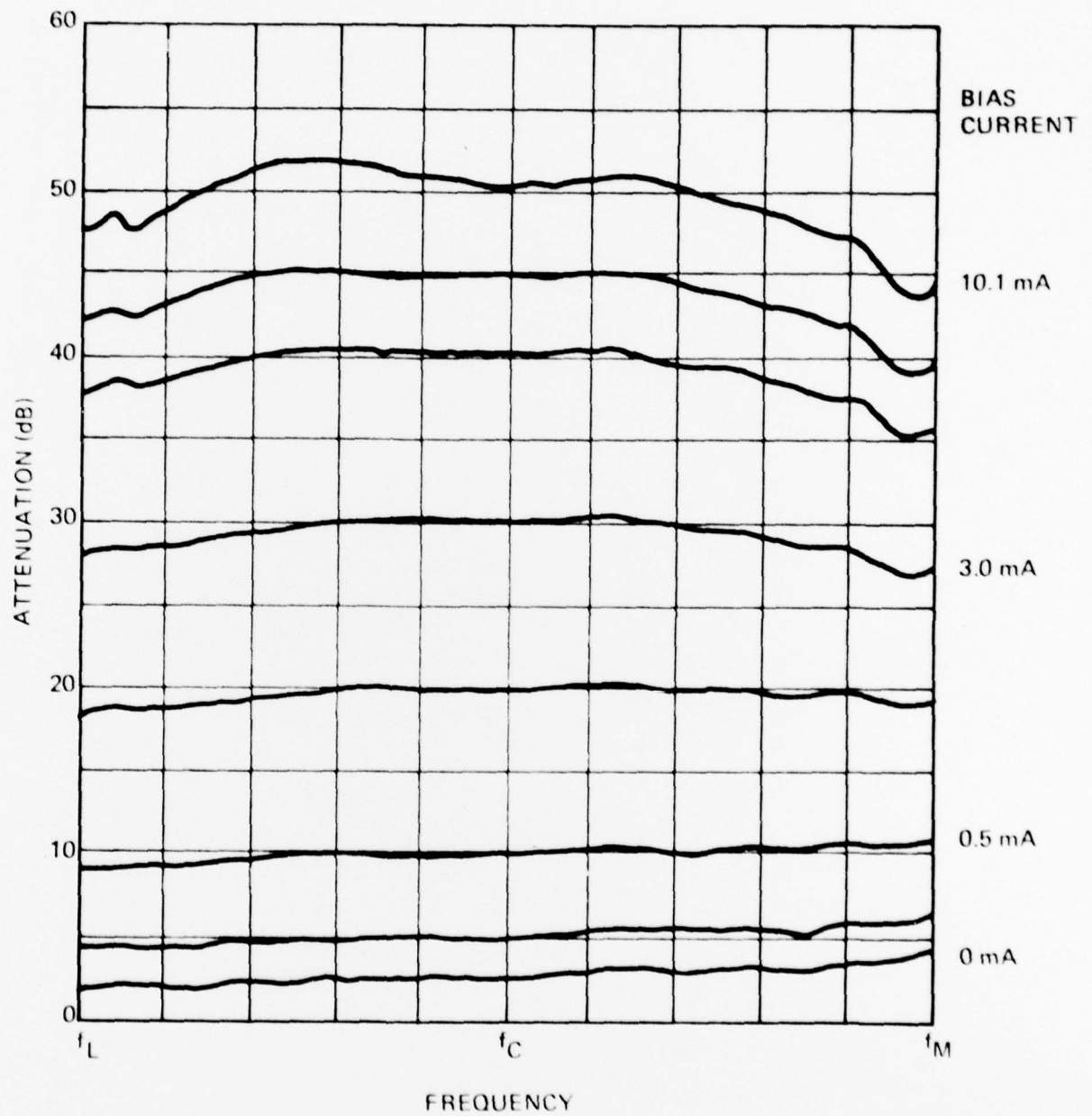


FIGURE 4.3.1 LINEAR AMPLITUDE MODULATOR ATTENUATION CHARACTERISTICS

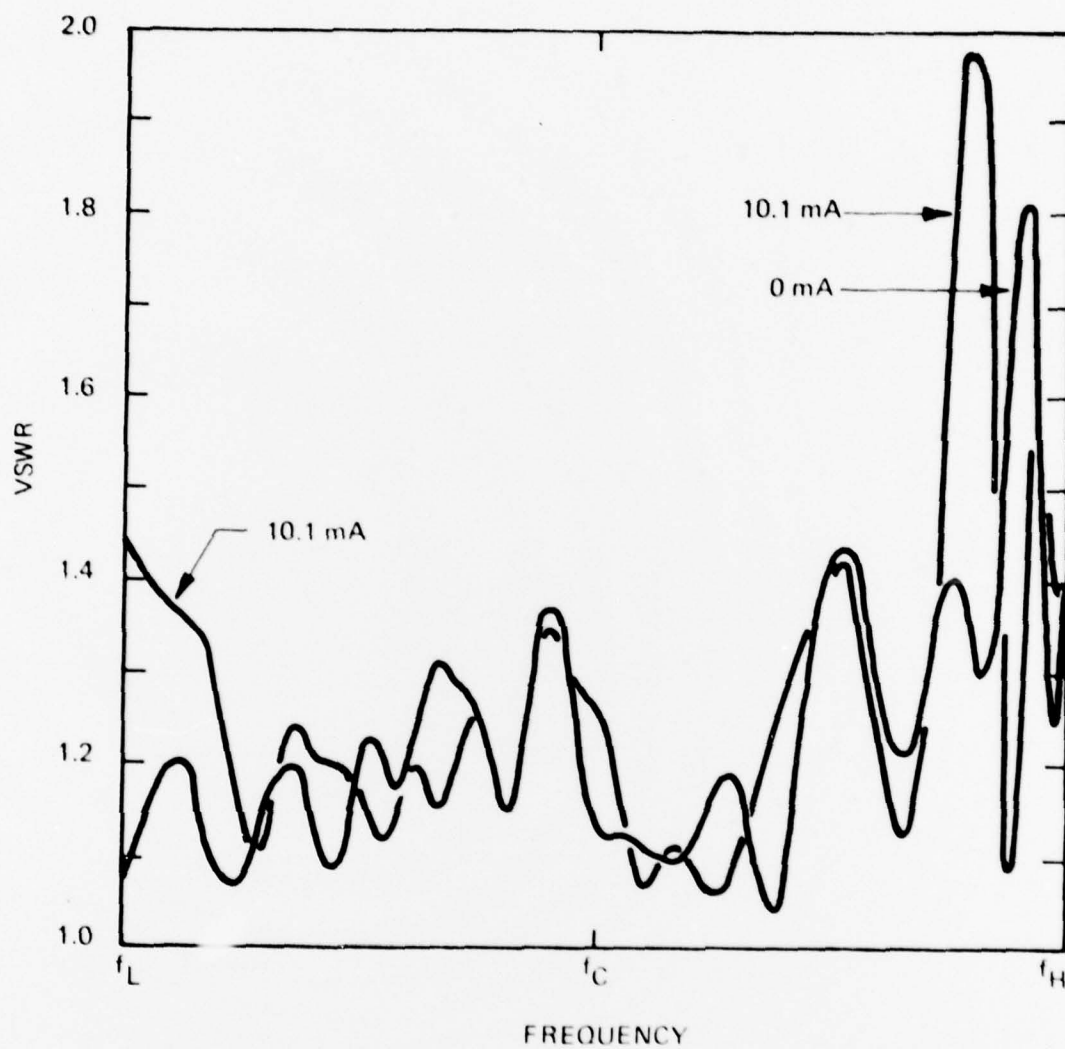


FIGURE 4.3.2 LINEAR AMPLITUDE MODULATOR VSWR CHARACTERISTICS

The 45 dB dynamic range is achieved at the 10.1 mA drive level except at the very top of the band, where it dips to about 40 dB. The VSWR is also well behaved, under 1.5, except in the same high frequency region, where it has a sharp spike which depends on the attenuation level. We suspect that these anomalies are due to low-Q resonances between two or more discontinuities, rather than radiation or higher order modes. However, this is conjecture and the problem bears further investigation.

Figures 4.3.3 and 4.3.4 illustrate the attenuation linearity. The first shows the attenuation above insertion loss versus command voltage at the center and band edge frequencies. The second gives the difference between the actual attenuation and a linear ramp at the center frequency. The peak deviation from linear is 1.8 dB, which is greater than the ± 1.0 dB desired, but about the same as achieved on the low band unit, up to the same attenuation level.

The switching transient between minimum and maximum loss states is shown in Figure 4.3.5. The leading edge, turn-off, switching time is 60 ns to the 90 percent point, including driver delay and approximately 100 ns to 100 percent attenuation. The trailing edge returns to the 3 dB level in 60 ns.

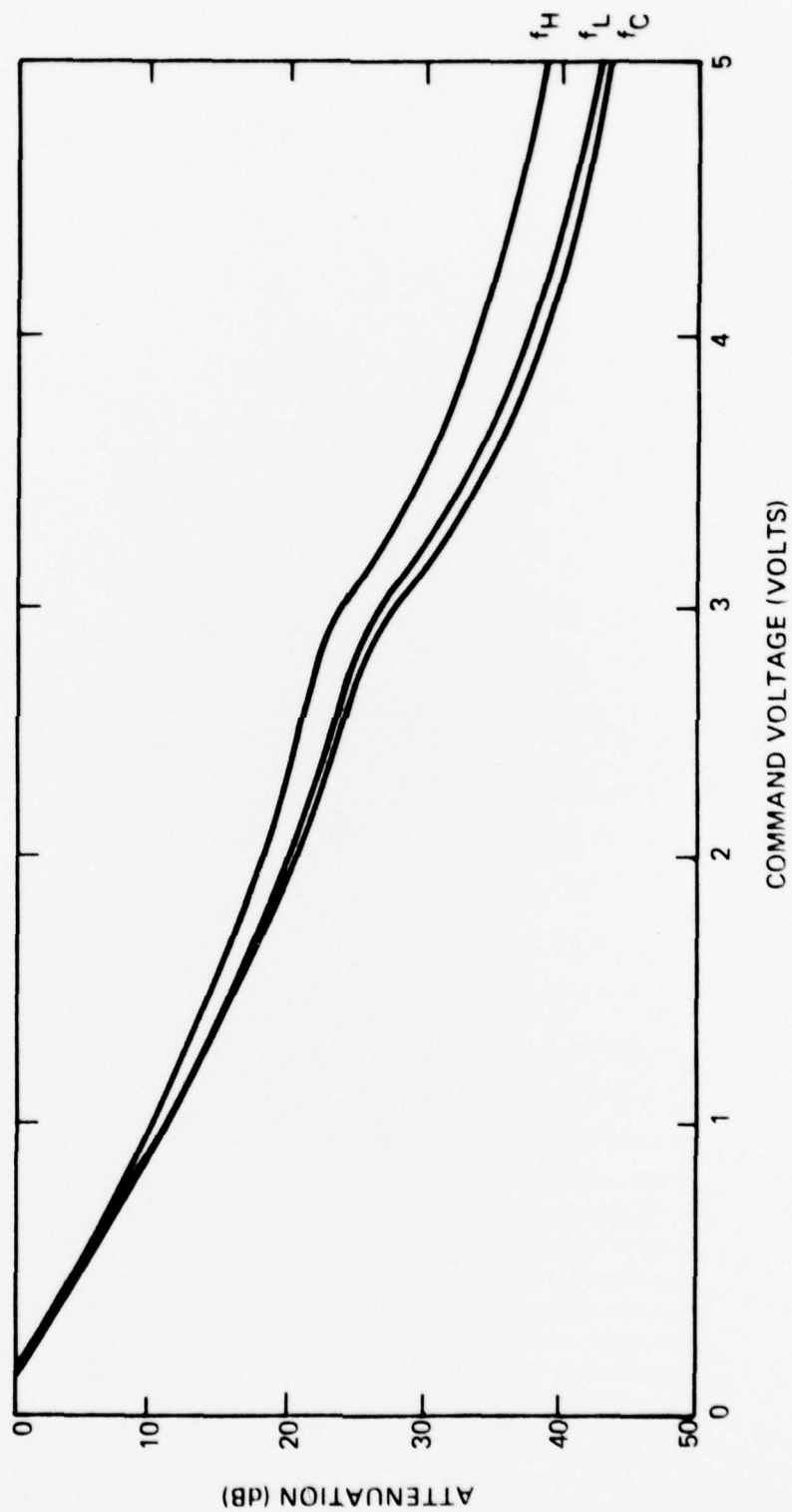


FIGURE 4.3.3 LINEAR AMPLITUDE MODULATOR ATTENUATION VS. DRIVER SIGNAL

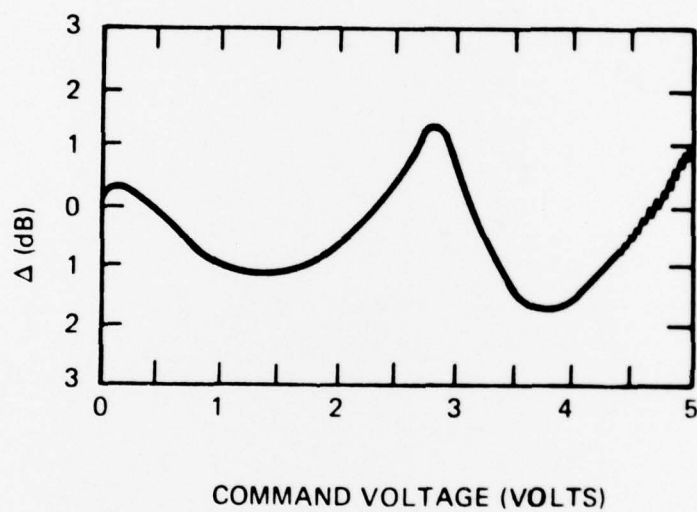


FIGURE 4.3.4 LAM LINEARITY ERROR VS. DRIVER INPUT VOLTAGE

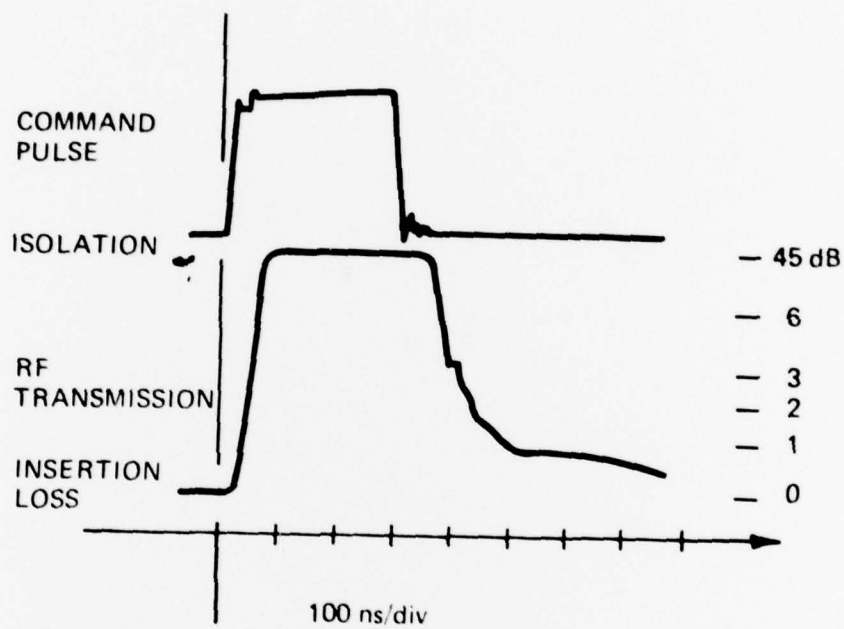


FIGURE 4.3.5 LAM SWITCHING TRANSIENT

5. CONCLUSIONS AND RECOMMENDATIONS

On the frequency translator, all of the basic performance specifications were met and the more optimistic 10 dB conversion loss goal was met for the lower 80 percent of the band. Toward the high end of the band there is some spurious or excess loss which we were unable to identify and correct, and which contributes about 1 dB to the conversion loss.

We found it essential to make the 3-dB hybrids on .015" alumina in order to obtain coupling and directivity characteristics in accord with design expectations. Apparently thicker (.020") substrates suffer from higher order modes or radiation problems. We also concluded early in the development that the directivity requirements could not be readily met with a stripline hybrid.

The microstrip power divider on .020" alumina worked excellently and it was not necessary to go to .015" material. We suspect that the reason for this is that the power divider topology is such that higher order modes are not readily excited, whereas the coupler, which must generate the coupled-line even and odd mode field configurations, tends also to generate other spurious modes.

We concluded that etching the power divider resistors right on the microstrip substrate is a very desirable technique from the cost and assembly point of view, even though we did not observe any significant performance improvement over the chip resistor model.

The performance of first trial stripline power dividers was totally unacceptable, and we abandoned that approach immediately.

We would recommend that further development of the high band translator be addressed to two areas which should improve the high frequency conversion loss by 1.5 to 2 dB. First, the high frequency loss mechanism should be identified and eliminated. Second, the output of the baseband modulator could be waveshaped such as to make the diode reflection coefficient versus drive amplitude be more nearly sinusoidal in time over a wider range. A single breakpoint linearizer-type circuit would probably work quite well.

The performance of the linear modulator was generally excellent over the lower 60-80% of the band. It falls slightly short of the design goals in insertion loss, flatness, and dynamic range at the upper end, primarily due to the excess loss mentioned in the frequency translator discussion, and also possibly due to spurious resonance effects.

We expect that the source of the high frequency losses of both the translator and modulator are the same and that solving the problem for one solves it for both.

The linearity deviation is greater than desired. We recommend that the driver be redesigned to include two breakpoints, to improve the linearity.

Since the maximum input power level for the high band modulator is much lower than that of the low band unit, we recommend that thinner I-layer diodes be tried to increase the switching speed. This may require some adjustments in the driver circuits. Therefore the work should be done in conjunction with the addition of another breakpoint.